

Stateresolved photodissociation of OCS monomers and clusters

N. Sivakumar, G. E. Hall, P. L. Houston, J. W. Hepburn, and I. Burak

Citation: *The Journal of Chemical Physics* **88**, 3692 (1988); doi: 10.1063/1.453869

View online: <http://dx.doi.org/10.1063/1.453869>

View Table of Contents: <http://scitation.aip.org/content/aip/journal/jcp/88/6?ver=pdfcov>

Published by the [AIP Publishing](#)

Articles you may be interested in

[State-resolved translation energy distributions for NCO photodissociation](#)

J. Chem. Phys. **114**, 9020 (2001); 10.1063/1.1369132

[An investigation of the 355 nm photodissociation of NO₂ by stateresolved photofragment imaging](#)

J. Chem. Phys. **99**, 4455 (1993); 10.1063/1.466072

[Quantum stateresolved study of the rovibrational excitation of OCS by hot hydrogen atoms](#)

J. Chem. Phys. **92**, 1687 (1990); 10.1063/1.458050

[Time and stateresolved measurements of nitric oxide dimer infrared photodissociation](#)

J. Chem. Phys. **89**, 1966 (1988); 10.1063/1.455694

[Stateresolved photofragmentation of OCS and CS₂](#)

AIP Conf. Proc. **146**, 497 (1986); 10.1063/1.35924



State-resolved photodissociation of OCS monomers and clusters

N. Sivakumar, G. E. Hall, and P. L. Houston

Department of Chemistry, Cornell University, Ithaca, New York 14853

J. W. Hepburn

Center for Molecular Beams and Laser Chemistry, University of Waterloo, Waterloo, Ontario N2L 3G1, Canada

I. Burak

School of Chemistry, Sackler Faculty of Science, Tel-Aviv University, Tel-Aviv, Israel

(Received 28 July 1987; accepted 9 December 1987)

Photodissociation of OCS in the region from 222–248 nm has been investigated by monitoring the CO and S(1D_2) primary photoproducts; as well as the secondary production of S(3P_2), S(3P_1), and S(3P_0) using fluorescence induced by a tunable vacuum ultraviolet laser source based on four-wave mixing in magnesium vapor. The quantum yield of S(3P) was found to be 0.00 ± 0.02 at 222 nm. Thus, in contrast to our preliminary report, the present more detailed investigation shows that the sole sulfur product appears to be S(1D). The CO photofragment is produced almost exclusively in $v = 0$ [$\text{CO}(v = 1)/\text{CO}(v = 0) \leq 0.02$], but the rotational distribution is inverted and peaked at very high rotational levels. The peak shifts from $J = 56$ for dissociation at 222 nm to $J = 31$ at 248 nm. Doppler profiles of the CO rotational transitions reveal (1) that all observed levels are produced in coincidence with S(1D), (2) that for 222 nm photolysis the fragment recoil anisotropy shifts from a distribution characterized by $\beta = 1.9$ at $J = 67$ toward one characterized by $\beta = 0$ near $J = 54$, (3) that the CO velocity vector is aligned nearly perpendicular to its angular momentum vector, and (4) that the CO angular momentum vector is also aligned parallel to that component of the transition dipole which lies perpendicular to the recoil velocity. These results are interpreted in terms of a model for the dissociation in which excitation takes place to two surfaces of A' and A'' symmetry derived from a bent $^1\Delta$ configuration. Dissociation of OCS clusters was also investigated and was found to produce a photochemistry completely different from that of the monomers. Rotationally cold CO as well as S₂ in both the $X^3\Sigma_g^-$ and $a^1\Delta_g$ states was observed.

I. INTRODUCTION

The understanding of photodissociation dynamics in small molecules has increased dramatically in the past few years, particularly for triatomic or pseudotriatomic species. A formal theory of such photodissociations has been developed,¹ and both theoretical and experimental studies have probed several important systems. Examples include the extensive studies of dissociation in ICN^{2–20} and CH₃I,^{21–33} where branching between the I*($^2P_{1/2}$) and I($^2P_{3/2}$) channels is of particular interest; the very detailed examinations of the dissociation of water, with emphasis on both ground^{34–37} and excited^{38–42} state OH products; and the comprehensive studies of H₂CO.^{43–55} Despite the rapid progress, much work remains. While theory¹ relates the dissociative potential energy surface to experimental cross sections through transition matrix elements, major experimental efforts are still needed to measure the cross sections for dissociation in sufficient, unaveraged detail so that these elements can be determined. At the same time, one would like to study a family of similar parent compounds to learn the extent to which information from one system can be used to predict the behavior in another.

The set of the isoelectronic molecules CO₂, OCS, and CS₂ is an attractive target of investigation. Firstly, the spectroscopy of these molecules has been studied extensively⁵⁶

and shows that they may be excited by absorption to electronic states of either linear or bent equilibrium geometries. Secondly, sufficiently intense laser sources have recently become available for photodissociation studies in the vacuum ultraviolet.^{57,58} Thirdly, the CO, CS, O, OH, and S fragments can all be probed sensitively, either by laser-induced fluorescence (LIF) or by multiphoton ionization (MPI).^{59–63} In the cases of OCS and CS₂ the heavy S atom contribution makes it possible to study the participation of triplet states in the dissociation process, reached either by direct absorption or by curve crossing from a singlet state.

Only a few studies of the CO₂ photodissociation have been reported, and these primarily concern the quantum yields for dissociation in the 1200–1670 Å region of the $^1\Delta_u \leftarrow ^1\Sigma_g^+$ transition. Early reports based on final product analysis concluded that the O₂/CO₂ ratio was less than the expected value of 0.5,^{64,65} but the discrepancy was later shown to be due to a surface phenomenon.⁶⁶ Attention then turned to the primary yield for CO₂ → CO + O(1D) photolysis. Inn⁶⁷ and Slanger *et al.*⁶⁸ suggested that the quantum yield for CO + O(1D) might be less than unity, but Slanger and Black⁶⁹ later demonstrated that the CO deficiencies observed in previous work could again be accounted for by heterogeneous processes. Thus while it is clear that CO and O(1D) are the primary photolysis products, there are still no reports of the internal energy distribution for the CO prod-

uct. Preliminary results from our own laboratory suggest that the CO is formed primarily in $v = 0, 1,$ and 2 with substantial rotational excitation.⁷⁰

In CS_2 , the corresponding $^1\Delta_u$ state is below the $\text{CS} + \text{S}(^3P)$ dissociation threshold, and so no photochemistry is possible following absorption of light on the $^1\Delta_u \leftarrow ^1\Sigma_g^+$ transition between 300–240 nm. On the other hand, photodissociation following excitation on the $^1\Sigma^+ \leftarrow ^1\Sigma_g^+$ transition in the 180–210 nm region has been extensively studied by several investigators.^{71–87} There is general agreement that the CS photoproduct is highly vibrationally excited, and there is also an indication of a high degree of rotational excitation. There is considerable controversy in the literature about the branching ratio between the $\text{S}(^1D)$ and $\text{S}(^3P)$ channels, with values for the $\text{S}(^3P)/\text{S}(^1D)$ ratio ranging from 0.25 to 6.0. Recent direct measurements have determined this ratio to be $\text{S}(^3P)/\text{S}(^1D) = 2.8$ and have also enabled a separation of the CS vibrational distribution into contributions from the two electronic channels.⁸⁷

The photodissociation of OCS on the $^1\Delta \leftarrow ^1\Sigma$ band near 222 nm has received extensive investigation, partly because OCS has been implicated in the atmospheric sulfur cycle.^{88–90} The increase in the OCS absorption coefficient with temperature has been used by four groups in assigning the geometry of the upper state to a bent configuration.^{91–94} Zittel and his co-workers^{95,96} have exploited this effect in the two-step photodissociation of OCS to separate O, C, and S isotopes. However, while product yields have been investigated for dissociation at shorter wavelengths,^{97–100} the only report of an internal energy distribution for dissociation near 222 nm is based on the observed temperature increase following photolysis,¹⁰¹ no detailed distributions have been measured.

In this paper we present the results of state-resolved photodissociation of OCS at wavelengths in the range 220–

250 nm. Excitation in this spectral region could lead to both $\text{S}(^3P)$ and $\text{S}(^1D)$:



where the indicated energies are for 222 nm dissociation. Preliminary results of our study at this wavelength have been reported earlier.^{102,103} The $\text{S}(^1D)/\text{S}(^3P)$ branching ratio, the internal state distribution of the CO, the angular distribution of fragment recoil, and the correlation of the CO rotational vector, the recoil velocity vector, and the transition dipole moment of the OCS parent compound are presented in this report. These vector correlations show that excitation of OCS takes place to both the A' and A'' components of the $^1\Delta$ Renner–Teller pair.

In addition to studies of the OCS monomer, results for 222 nm dissociation of $(\text{OCS})_n$ clusters ($n = 2–8$) are described. Photodissociation of the clusters leads to a photochemistry which is completely different from that of the monomer. S_2 as well as rotationally, vibrationally, and translationally cold CO photoproducts are observed. Photodissociation of OCS clusters provides one of the few cases^{104–107} in which a photochemical reaction has been observed to occur between weakly bound members of a van der Waals cluster.

II. EXPERIMENTAL

A schematic diagram of the experimental apparatus is shown in Fig. 1. Briefly, OCS was seeded in helium and expanded in the nozzle system previously described.¹⁰⁸ Following photolysis of the OCS by a laser operating in the 220–250 nm range, the CO and S products were detected using tunable vacuum ultraviolet (VUV) laser-induced fluorescence (LIF).

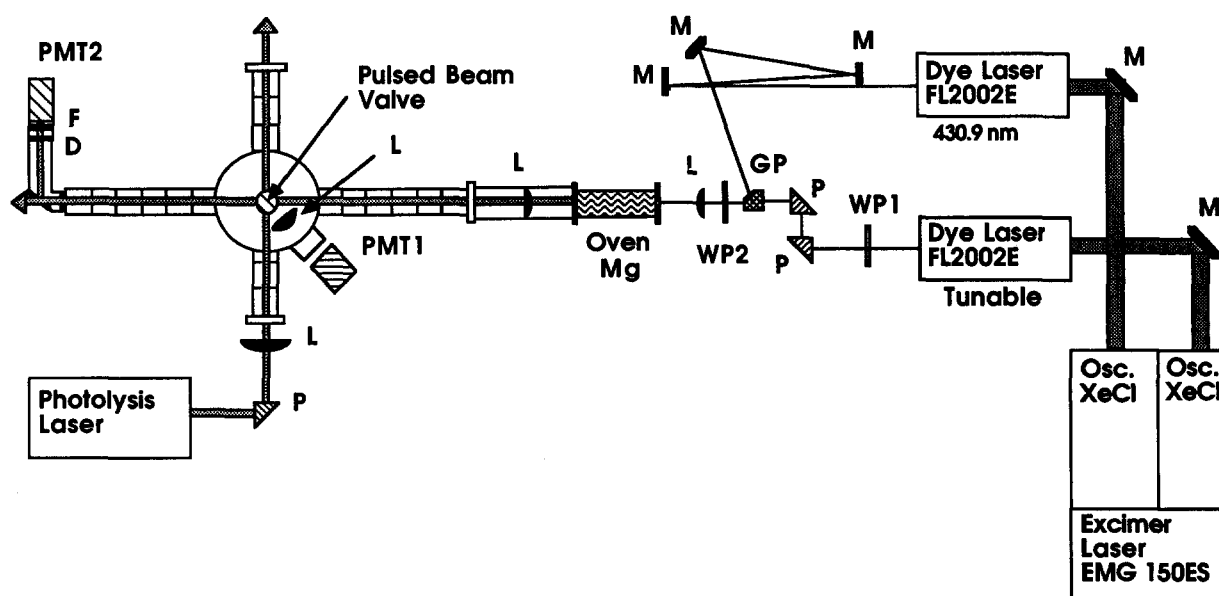


FIG. 1. Schematic diagram of the experimental apparatus. M: mirror, P: prism, WP: waveplate, L: lens, GP: glan prism, PMT: photomultiplier tube, D: diffuser, F: filter.

A. Molecular beam chamber

The nozzle expansion was achieved using a pulsed beam valve (Newport BV-100) with an orifice of 0.5 nm and a stagnation pressure of typically 25 psi. Pulse durations were on the order of 250 μ s (FWHM), and the background pressure in the chamber with the beam on was around 2×10^{-5} Torr. Usually, the photolysis mixtures were prepared by flowing He(99.9%) over OCS held at a specified temperature, but in some cases premixed samples were used in order to test how the signal varied with partial pressure of OCS. Although there was no convenient method for determining the rotational temperature of the expanded OCS, a 1:35 mixture of CO in He under the same nozzle expansion conditions was found to have a 30 K rotational temperature.

The photolysis and probe laser beams and the molecular beam propagated along mutually orthogonal directions and the lasers intersected each other and the molecular beam 25–40 nozzle diameters downstream from the orifice. The two laser beams entered and exited the beam chamber through long arms equipped with irises to minimize the scattered light. In the case of each laser beam, entrance and exit windows were mounted perpendicular to the propagation direction. Laser-induced fluorescence was viewed through a LiF window at 45° to the laser beams using a single 1.5 in. focal length lens (MgF₂) for collection. An aperture of 3/8 in. diameter placed just in front of the LiF window limited the viewing region in the chamber to approximately 2–3 mm in diameter.

B. Probe laser

Laser-induced fluorescence was used to probe the vibrational and rotational populations of the CO product on the ($A^1\Pi \leftarrow X^1\Sigma^+$) system and to probe the S(¹D) and S(³P) products on a variety of atomic transitions. The VUV required for these measurements was generated by two-photon resonantly enhanced four-wave sum mixing in magnesium vapor,¹⁰⁹ a technique which has previously been used in a variety of experiments.^{110–112} The oscillator and amplifier sides of a dual-cavity XeCl excimer laser (Lambda Physik EMG 150ES) were configured as two synchronized oscillators to pump two dye lasers (Lambda Physik FL 2002E). The pulse duration and linewidth for each dye laser were approximately 15 ns and 0.25 cm^{-1} (FWHM), respectively, and each dye laser produced light of vertical polarization. One of dye lasers was fixed in wavelength at 430.9 nm on the two-photon transition ($3s3d^1D - 3s^2^1S$) in magnesium, while the second dye laser was scanned. By using several days in the scanned laser, the VUV could be tuned between 140 and 170 nm. Typical pulse energies were 5 mJ for the fixed frequency laser and 15 mJ for the scanned laser.

The two beams were overlapped in time by using a fixed optical delay of 16 ns for the fixed frequency laser and by then varying the buffer gas pressure in one of two pump laser cavities in order to maximize the VUV output. The two laser beams were spatially overlapped by combining them in a Glan prism. The polarization of one of the beams was rotated to the horizontal direction by the use of a $\lambda/2$ plate; a $\lambda/4$ plate was then used following the Glan prism to make the beams circularly polarized in order to suppress third har-

monic generation of the fixed frequency light.¹¹³ As a consequence, the VUV output was also circularly polarized.

The two beams were focused into a magnesium oven by a 10 in. quartz lens and recollimated by a MgF₂ lens placed after the oven. LiF wedges (0.5°) were used on the output side of the oven and on the entrance and the exit sides of the beam chamber in order to avoid possible etalon effects. The dye laser beams were transmitted together with the VUV beam through the chamber. The VUV was monitored during the course of the experiment with a solar-blind photomultiplier tube (PMT2, EMI G-26E314LF) by taking a reflection from a LiF window mounted at 45° to the probe beam. The reflection passed through a MgF₂ diffuser and a VUV band pass filter (Acton 140-B) before reaching the photocathode of the PMT. The transmission of the filter changes by less than 3% in the wavelength region of the experiments, and no correction was made for this variation.

The linewidth of the VUV was $\approx 0.7 \text{ cm}^{-1}$ (FWHM) during normal operation. For Doppler profile measurements, air-spaced intracavity etalons were used in both dye lasers, and the tuned dye laser was scanned by ramping the N₂ pressure in the etalon/grating chamber. The resulting VUV linewidth was $\approx 0.16 \text{ cm}^{-1}$.

The VUV output energy was not measured, but from spectra of CO taken at known pressures we estimate a sensitivity limit (S/N = 1) of 10^6 – 10^7 molecules cm^{-3} per quantum state.

For probing of the S₂ product, the output of the un narrowed dye laser pumped by the amplifier side of the excimer laser was frequently doubled using KDP crystals.

C. Photolysis laser

Several photolysis sources were used, depending on the desired photolysis wavelength. At 222 nm, an unpolarized KrCl excimer laser (Lumonics TE861-4) was used as the photolysis source in measurements of the CO vibrational and rotational distributions. This laser was triggered by a spark gap and had a jitter of 50 ns. At 248 nm, a KrF excimer laser was employed (Lambda Physik EMG101), while at 235 nm the doubled output of a dye laser pumped by a Nd:YAG laser was summed with the fundamental (Quanta Ray DCR-2A/PDL-1/WEX-1). This latter system was also used for Doppler profile measurements at 222 nm. This output beam could be either horizontally or vertically polarized, depending on the configuration of an S1-UV quartz beam-steering periscope. At all wavelengths, the photolysis energy was monitored during the course of the experiment using a photodiode to view the fluorescence from a dye cell illuminated by a reflection of the photolysis beam after transmission through the beam chamber. Typical photolysis energies were in the range 0.5–1.5 mJ/p, except at 248 nm where approximately 10 mJ/p was available. The photolysis beam was weakly focused using a 75 cm lens with the focus 15 cm beyond the center of the chamber.

D. Detection electronics

Fluorescence detection of CO was accomplished using a solar-blind photomultiplier tube (PMT1, EMR 541G-09-17), while fluorescence detection of S₂ was accomplished

using a UV sensitive photomultiplier (Hamamatsu R928) equipped with filters for rejection of scattered photolysis light. In either case, the fluorescence signal, the probe laser intensity, and the photolysis laser intensity were each averaged (typically ten shots) by gated integrators (SRS, Model SR250) using apertures longer than the fluorescence signals. The outputs were digitized and fed to a computerized data acquisition system (LSI 11/23) that also scanned the probe laser and, in the case of S₂ detection, angle tuned the doubling crystal.

The two integrators which averaged the signal and the probe laser intensity were triggered by a photodiode viewing fluorescence from the amplifier dye cell of one of the dye lasers. Timing was controlled by a home-built trigger generator operating at 10 Hz. A delay of typically 200 ns between the probe and photolysis lasers was used during spectral scans, and a delay of 100 ns was used during Doppler profile measurements. When the spark-gap-triggered excimer laser was employed, the time resolution was approximately 50 ns; it was nearly a factor of two better for the other photolysis sources. Scans of the time delay between the photolysis and probe lasers were accomplished with the scanning gate feature of a PAR 162 boxcar averager, using one channel's gate output to trigger the probe laser and the other channel to monitor the signal with a synchronously scanned gate.

E. Chemicals

OCS was obtained from Matheson at a stated purity of 96%. The sample was subjected to freeze-pump-thaw cycles at liquid N₂ temperature many times to remove the CO present. Less volatile impurities, such as CS₂, were reduced by simple distillation from the sample reservoir, typically held near 179 K in a methanol slush bath during the experiments.

III. RESULTS AND DISCUSSION

A. Quantum yield for the singlet and triplet sulfur channels

It is possible to detect the atomic S(¹D) and S(³P) products from OCS fragmentation by LIF using VUV tunable in the same spectral region used to probe CO. The following transitions were used to detect ¹D₂ and ³P_J sulfur atoms¹¹⁴

$${}^1P_1^0 \leftarrow {}^1D_2 \quad 69\,051 \text{ cm}^{-1}, \quad (3)$$

$${}^3D_3^0 \leftarrow {}^3P_2 \quad 67\,843 \text{ cm}^{-1}, \quad (4)$$

$${}^3D_2^0 \leftarrow {}^3P_1 \quad 67\,429 \text{ cm}^{-1}, \quad (5)$$

$${}^3D_1^0 \leftarrow {}^3P_0 \quad 67\,243 \text{ cm}^{-1}. \quad (6)$$

Figure 2 displays a temporal scan of the three S(³P_J) levels following dissociation of a bulb sample of OCS at 1 mTorr in 5 Torr of He. The three signals were placed on an absolute scale by observing the signal level at much longer times after Boltzmann equilibrium had been attained. The initial spike in each scan is due to scattered photolysis light, but the very low signal level immediately following this spike suggests that there is little, if any, S(³P) produced as a primary photoproduct. The S(³P) signals then rise rapidly due to efficient quenching of translationally excited S(¹D₂) atoms by the He/OCS mixture and then more slowly due to quenching of thermalized S(¹D₂).

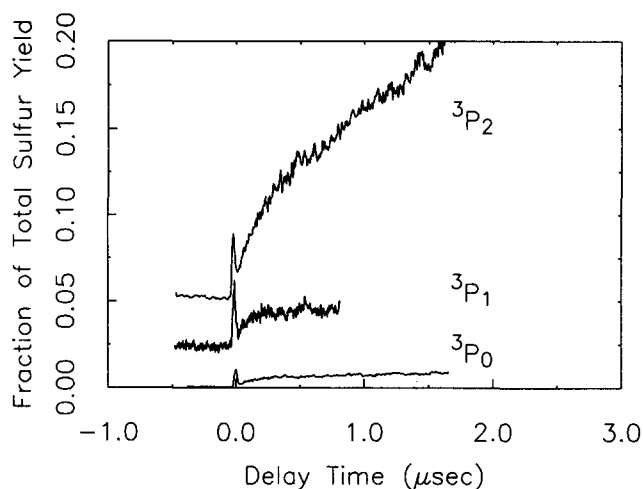


FIG. 2. Laser-induced fluorescence of the S(³P_J) levels as a function of delay time between the photolysis and probe lasers following dissociation of a bulb sample of OCS at 1 mTorr in 5 Torr of He.

The interpretation of Fig. 2 needs to be approached with some caution. First, since the boxcar gate opens slightly after the firing of the probe laser, the zero in time difference between the two laser pulses is actually slightly delayed from the spike caused by scattered photolysis light. Nonetheless, the S(³P) signals do not appear to rise instantaneously; they start from a level near zero and then display a relatively rapid rise followed by a much slower rise. The rapid rise cannot be attributed to an instantaneous rise convoluted with the time resolution of the measurement, determined primarily by the laser pulsewidths and the jitter between the two lasers. The time resolution of the experiment is at least as fast as that indicated by the width of the scattered light, and this initial spike in the trace is itself much shorter than even the fast portion of the rise in any S(³P) signal. We thus conclude that the S(³P) is detected with adequate time resolution and that there is little, if any, S(³P) produced directly by the photodissociation. From the observed signals, we estimate that the upper limit to S(³P) production is 2%. We note that if the resolution of the experiment had been determined by a time constant greater than about 100 ns, then the fast rise in the S(³P) signals might have appeared to be initial triplet formation. This fact appears to have influenced previous results, as discussed in below. The kinetics of the quenching process and the branching of quenching among the S(³P) levels will be reported in a separate communication.¹¹⁵

Previous measurements of the relative yields for the S(¹D) and S(³P) channels have led to some controversy. The yield of the S(³P) channel has been determined by chemical trapping methods at 229 nm to be 0.24 with a total dissociation yield of 0.9.^{91–92} However, a more recent study in which the S(³P) product from 248 nm dissociation was monitored by direct two-photon laser-induced fluorescence contends that the yield is likely to be zero, although the data admit the possibility that it might be as high as 0.15.¹¹⁶ Our measurements indicate that an upper limit to yield for the S(³P) channel is 0.02, assuming the quantum yield for disso-

ciation to be unity. That this measurement is at variance with our previous determination¹⁰² of 0.15 ± 0.05 deserves comment. First, the apparent triplet yield is strongly affected by how carefully and recently the OCS is distilled; CS₂ impurities, which would yield S(³P) on dissociation,⁸⁷ are the principal concern. A second problem is that some of our previous measurements were performed on beam samples, where cluster dissociation might contribute to the yield. Dissociation of OCS clusters does produce prompt S(³P₂). But the most important problem is evident in Fig. 2. The S(³P) signals rise very rapidly, even when inefficient quenchers such as He are used to limit diffusion (see Fig. 2). In the presence of larger laser scatter or low time resolution, this rapid rise, which is apparently caused by efficient quenching of translationally excited S(¹D),¹¹⁵ can easily be mistaken for prompt triplet yield. When greater effort is made to remove laser scatter and improve the time resolution, it becomes apparent that there is little initial production of S(³P); i.e., the quantum yield for S(¹D) is nearly 1.0. This result is in quite close agreement with that obtained by the two-photon laser-induced fluorescence method¹¹⁶ and it appears that the chemical trapping method overestimates the triplet yield, probably because quenching of the S(¹D) occurs on the time scale of the trapping.

B. The CO fragment

1. Experimental results

The internal state distribution of the CO fragment produced by photodissociation of OCS at 222, 235, and 248 nm was measured using vacuum ultraviolet laser-induced fluorescence. Figure 3 shows the LIF spectrum of the (3,0) band of the CO (*A* ← *X*) system following OCS dissociation at 222 nm. Similar data, although with lower signal-to-noise ratio, were obtained on the (2,0) and (3,0) bands following dissociation at 235 and 248 nm, respectively. Despite extensive searches in the regions of the (4,1) and (3,1) bands, no lines were observed which could be attributed to absorption

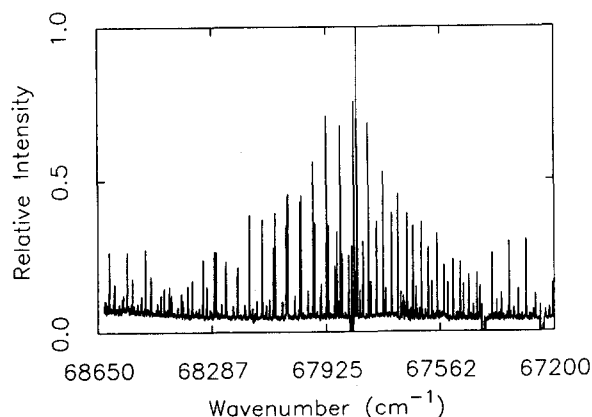


FIG. 3. Laser-induced fluorescence spectrum of the (3,0) band of the CO photoproduct following dissociation at 222 nm of a beam of 3% OCS in He. The delay time between the photolysis and probe lasers was 200 ns. The sulfur transitions have been reduced by a factor of 10 to bring out the CO features.

from CO(*v* = 1). From the signal-to-noise ratio of the spectrum we estimate that $N(v = 1)/N(v = 0) \leq 0.02$ at 222 nm, and ≤ 0.06 at 235 nm.

In order to record a complete spectrum of the (3,0) band for the highly rotationally excited CO photoproducts, the tuned dye laser was scanned from 450–481 nm corresponding to VUV wavelengths from 146–149 nm. Possible systematic drifts in sensitivity over this broad spectral range were avoided by frequent recording of a series of CO photoproduct reference lines. These reference lines were then used to normalize the various segments of the CO spectrum before they were combined. For the spectra analyzed in this study, the normalization factors were always found to be 1.0 ± 0.1 .

Peak heights of the rotational lines were used for extracting the relative populations of internal states following verification that this procedure gave results equivalent to the use of integrated areas. From the measured intensity, $I_{J', J''}$, of a line in a given vibrational band, the relative rotational state population is given by

$$P(J'') \propto I_{J', J''} (2J'' + 1) / (v S_{J', J''}), \quad (7)$$

where the relevant Hönl–London factors $S_{J', J''}$ for the *P*, *Q*, and *R* branches are taken from the literature.¹¹⁷ Rotational distributions for the CO(*v* = 0) produced by dissociation at the three wavelengths are displayed in Fig. 4. These distributions are uncorrected for the variation in product alignment with rotational level. For the case of 222 nm dissociation, this variation has been measured by analysis of the Doppler profiles, as will be described later.

Dissociation at 222 nm results in a CO rotational distribution that is sharply peaked at $J = 56$ with a subsidiary maximum at $J = 67$. The rotational distribution produced by 235 nm photolysis is very similar in shape to that from 222

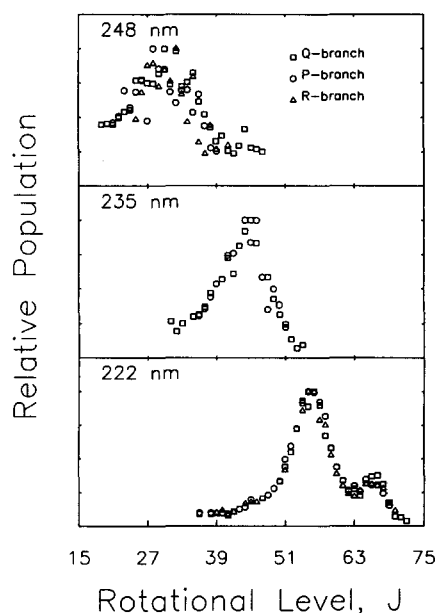


FIG. 4. Rotational distributions of CO(*v* = 0) produced by photodissociation of OCS at different wavelengths. (a) 248 nm, (b) 235 nm, (c) 222 nm.

nm photolysis except that the peak of the distribution is shifted to lower J ($J \approx 46$), and no secondary maximum is observed. The absorption coefficient of OCS is very small at 248 nm, which results in a small signal-to-noise ratio for the CO photoproduct spectrum. In spite of this fact, it is possible to determine that the peak of the distribution shifts to approximately $J = 30$. The average energy in rotation, $\langle E_{\text{rot}} \rangle$, in cm^{-1} and the average rotational energy level, $\langle J \rangle$, at each of the three dissociation wavelengths was found to be: 222 nm: 6200, 57; 235 nm: 3900, 45; 248 nm: 2000, 32. Expressed as fractions of the available energy, the results indicate that 58%, 47%, and 33% of the available energy appears in rotation for dissociation at 222, 235, and 248 nm, respectively.

Doppler profiles of many of the rotational lines were measured following 222 nm photolysis in order (1) to separate the contribution of the two channels at each particular J and (2) to determine the anisotropy of fragment recoil vectors as a function of the CO internal energy level. A third reason for the Doppler investigation, which only became evident following examination of the data, was that analysis of the how the Doppler profile of the same CO(J) level varies with Q or P, R transitions and with excitation/detection geometry provides information on the angular correlation between the velocity and angular momentum vectors. Figure 5 displays the Doppler profiles for a selection of CO(J) levels for different probe transitions and for different polarization configurations. The data and the smooth curves will be discussed below.

2. CO internal energy distribution

For the wavelengths at which the dissociation has been studied, no vibrationally excited CO fragment was observed,

and an upper limit of $(N_{v''=1}/N_{v''=0}) \leq 0.2$ was obtained at 222 nm. The properties of the CO bond in the OCS molecule are very similar to those of the free CO diatomic molecule. The C–O bond distance in OCS is 1.116 Å compared to 1.128 Å in CO. The symmetric stretch frequency in OCS is 2079 cm^{-1} , whereas the vibrational frequency of CO is 2169.8 cm^{-1} . In a simple Franck–Condon model^{118–120} for a collinear dissociation, the population of the CO product in vibrational level v is proportional to the square of the overlap integral between the wave function of the ground state OCS molecule and that for CO in level v . Since there is only a very small change in the CO bond properties between OCS and CO, there will be substantial overlap for $v = 0$ and little overlap for other vibrational levels. Thus, it is not surprising that CO is not observed in excited vibrational levels.

The rotational distributions measured for $v'' = 0$ of CO are shown in Fig. 4(a)–4(c). These distributions are uncorrected for variations in alignment among the rotational levels. For 222 nm photolysis, the alignment factors have been determined at each rotational level using a linearly polarized photolysis source as described later and are listed in Table I where $\beta_0^2(02) = (5/4)A_0^2$. The rotational distributions shown in Fig. 4(a) were obtained using an unpolarized KrCl laser, so that the alignment is reduced by a factor of 2. The correction of the populations for alignment can be calculated using Eq. (1) of Greene and Zare.¹²¹ The corrections are relatively small; in the worst case the correction is 13%.

It is interesting to note that the high degree of CO rotational excitation cannot be predicted by any simple impulsive model in which a force acts between the separating sulfur and carbon atoms in a bent OCS molecule. In such an explanation, the largest impact parameter for the half-collision would be the distance of the carbon from the CO center

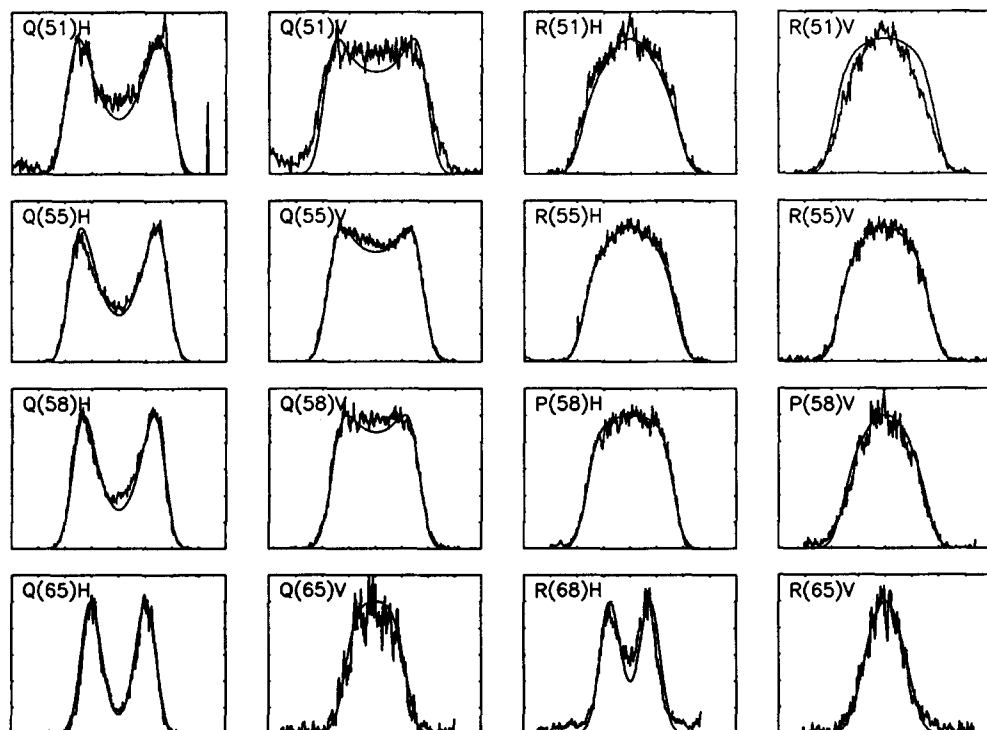


FIG. 5. Doppler profiles of representative CO(J) lines taken on different transitions and with different geometrical arrangements. $Q(J)$, $P(J)$, $R(J)$ represent the different branches; H represents horizontal geometry ($\theta' = 0^\circ$), while V represents vertical geometry ($\theta' = 90^\circ$). The smooth lines are the predicted profiles based on the model described in the text. The intensity along the ordinate of each panel is arbitrary; all profiles have been normalized to the same height. The scale on the abscissa is laser detuning from -0.5 to $+0.5 \text{ cm}^{-1}$.

TABLE I. Parameters used in Doppler fits

<i>J</i>	Data ^a	<i>f</i>	$\beta_0^2(20)$	$\beta_0^2(02)$	$\beta_0^0(22)$	$\beta_0^2(22)$	$\beta_0^2(42)$	$\beta_0^2(24)$	$\beta_0^0(44)$	$\beta_0^2(44)$	$\beta_0^2(64)$
50	<i>Qh, Qv</i> <i>Pv</i>	0.30	-0.050	0.549	-0.500	0.500	0.112	-0.237	0.375	-0.375	-0.106
51	<i>Qh, Qv</i> <i>Ph, Pv</i> <i>Rh, Rv</i>	0.30	-0.050	0.549	-0.500	0.500	0.112	-0.237	0.375	-0.375	-0.106
52	<i>Qh, Qv</i> <i>Pv</i>	0.33	-0.005	0.504	-0.500	0.500	0.086	-0.211	0.375	-0.375	-0.085
53	<i>Qh, Qv</i> <i>Ph, Pv</i> <i>Rh, Rv</i>	0.33	-0.005	0.504	-0.500	0.500	0.086	-0.211	0.375	-0.375	-0.085
54	<i>Qh, Qv</i> <i>Pv, Rh</i> <i>Rv</i>	0.35	0.025	0.474	-0.500	0.500	0.068	-0.193	0.375	-0.375	-0.071
55	<i>Qh, Qv</i> <i>Ph, Pv</i> <i>Rh, Rv</i>	0.38	0.070	0.429	-0.500	0.500	0.042	-0.167	0.375	-0.375	-0.050
56	<i>Qh, Qv</i> <i>Rh, Rv</i>	0.40	0.100	0.399	-0.500	0.500	0.025	-0.150	0.375	-0.375	-0.037
57	<i>Qh, Qv</i> <i>Ph, Pv</i> <i>Rv</i>	0.43	0.145	0.354	-0.500	0.500	-0.001	-0.123	0.375	-0.375	-0.016
58	<i>Qh, Qv</i> <i>Ph, Pv</i> <i>Rv</i>	0.46	0.190	0.309	-0.500	0.500	-0.028	-0.097	0.375	-0.375	0.004
59	<i>Qh, Qv</i> <i>Ph, Pv</i> <i>Rh, Rv</i>	0.50	0.250	0.249	-0.500	0.500	-0.063	-0.062	0.375	-0.375	0.032
60	<i>Qh, Qv</i> <i>Pv, Rv</i>	0.54	0.310	-0.189	-0.500	0.500	-0.098	-0.027	0.375	-0.375	0.059
61	<i>Qh, Qv</i>	0.60	0.400	0.100	-0.500	0.500	-0.150	0.025	0.375	-0.375	0.100
62	<i>Qh, Qv</i>	0.70	0.550	-0.050	-0.500	0.500	-0.238	0.113	0.375	-0.375	0.169
63	<i>Qh, Qv</i>	0.75	0.625	-0.125	-0.500	0.500	-0.281	0.156	0.375	-0.375	0.203
64	<i>Qh, Qv</i>	0.80	0.700	-0.200	-0.500	0.500	-0.325	0.200	0.375	-0.375	0.238
65	<i>Qh, Qv</i> <i>Rv</i>	0.90	0.850	-0.350	-0.500	0.500	-0.412	0.288	0.375	-0.375	0.306
66	<i>Qh, Qv</i>	0.95	0.925	-0.425	-0.500	0.500	-0.456	0.331	0.375	-0.375	0.340
67	<i>Rv</i>	0.98	0.970	-0.470	-0.500	0.500	-0.482	0.357	0.375	-0.375	0.361
68	<i>Rh, Rv</i>	0.95	0.925	-0.425	-0.500	0.500	-0.456	0.331	0.375	-0.375	0.340

^a*Q, P, R* indicate transition branch, *h* indicates $\theta' = 0$, *v* indicates $\theta' = 90$.

of mass, 0.638 Å. The recoil velocity of the CO fragment can be calculated from energy conservation for, say, $J = 60$ and 222 nm dissociation to be $v_{\text{CO}} = 1.27 \times 10^5$ cm/s. The relative velocity of the S and CO fragments is thus 2.38×10^5 cm/s, and the maximum orbital angular momentum, $L_{\text{max}} = \mu_{\text{OCS}} v_{\text{rel}} b_{\text{max}}$, is then $36 \hbar$, considerably less than the observed CO angular momentum ($J = 60$). For an impulsive

model to explain the observed rotation, the S atom would have to “push” against a point on the CO axis 0.425 Å further out from the CO center of mass than the location of the carbon atom. It seems more likely that the impulse approximation is incorrect and that the details of the trajectory on the dissociative surface are more complicated than predicted by this simple model.

The rotational distribution produced for dissociation at the shortest wavelength, 222 nm, has been considered in detail by Schinke.¹²² Analysis by his "rotation reflection principle" is based on an infinite-order sudden approximation to the photodissociation scattering amplitude. Since for the $S(^1D)$ channel the two peaks in the rotational distribution correspond to deposition of 58% and 80% of the available energy into rotation, it is not expected that the sudden approximation should provide an accurate description in this case. However, a modified version, in which conservation of energy is explicitly included, does produce fair agreement with the lower of the two peaks in the rotational distribution using a model potential surface. In particular, the calculation shows an asymmetric peak at $J = 55$ of similar width to that observed in Fig. 4(c). The subsidiary maximum at $J = 67$ was not reproduced by the calculation and was thought to be due to a special feature of the true potential.

The origin of this subsidiary maximum at $J = 67$ in the rotational distribution obtained for dissociation at 222 nm has received considerable attention. Because the ratio of this peak to the peak at $J = 55$ is in reasonable agreement with literature values of the $S(^3P)/S(^1D)$ ratio and because the $S(^3P)$ channel has more energy available for disposal in to internal degrees of CO, it was supposed previously¹⁰² that the subsidiary maximum corresponded to the CO from the 3P channel. However, as discussed in greater detail in Sec. III B 3, the widths of the Doppler profiles for rotational levels near $J = 67$ agree very well with the widths expected if CO in these levels is produced in coincidence with $S(^1D)$ and are some 40% narrower than those which would be expected if the CO were produced in coincidence with $S(^3P)$. For example, Fig. 6 displays the Doppler profile for the $R(67)$ line and the fits assuming that the $CO(J = 67)$ is produced in coincidence with $S(^1D)$ (solid line) or $S(^3P)$ (dashed line). (The shapes of the profiles will be described below; the widths, however, are determined solely by the internal ener-

gy of the sulfur atom.) It is clear from the figure that $CO(J = 67)$ is produced in coincidence with $S(^1D)$. Similar results were found for all rotational states for which Doppler profiles have been measured. Therefore, the subsidiary peak at $J = 67$ is not due to the $S(^3P)$ channel. In fact, we could find no Doppler profile with a width larger than that predicted for the $S(^1D)$ channel, a fact which corroborates our determination that the triplet yield is nearly zero.

The possibility that the subsidiary peak near $J = 67$ in the CO rotational distribution might be caused by dissociation of vibrationally excited OCS molecules has also been ruled out. Because the $^1\Delta - ^1\Sigma$ transition in OCS is forbidden except through vibronic coupling with the bending mode, those OCS molecules in the molecular beam which were not relaxed by the expansion from their first excited bending level will absorb much more strongly than OCS molecules in their ground vibrational level.^{92,93} Thus, a small fraction of vibrationally excited OCS could conceivably give rise to a disproportionate fraction of the CO product, and it might be presumed that this product would be more rotationally excited than the CO product from dissociation of ground state OCS. However, the Doppler measurements are not consistent with this explanation. The ν_2 bending quantum of OCS is at 520.4 cm^{-1} , so that $CO(J = 67)$ produced in coincidence with $S(^1D)$ should have a velocity of $10.37 \times 10^4 \text{ cm/s}$ if dissociation occurred from $OCS(\nu_2 = 1)$ and only $9.15 \times 10^4 \text{ cm/s}$ if dissociation occurred from ground state OCS. The experimental Doppler profiles fit the velocity corresponding to dissociation from the ground state, as shown by the solid line in Fig. 6, whereas the Doppler profile for dissociation from $\nu_2 = 1$ is definitely outside the error limits of the data, as shown by the dotted line in Fig. 6. It is conceivable that the uncertainty in the OC-S bond dissociation energy is as much as 520 cm^{-1} , so that an alternate dissociation energy might give a better fit to the $J = 67$ line for dissociation from $\nu_2 = 1$. However, *all* rotational levels from $J = 48-68$ were fit accurately with the same dissociation energy; there was no discontinuity in the fits between those for rotational levels in the two peaks of the rotational distribution.

As will be shown below, a strong case can be made on the basis of the shapes of the Doppler profiles that two peaks arise from dissociation via two different repulsive surfaces, one of A'' symmetry and one of A' symmetry.

3. Interpretation of Doppler line shapes: Angular distributions and vector correlations

The magnitude of the velocity v of a particular $CO(v, J)$ level can be determined by conservation of energy and linear momentum

$$v_{CO}(0, J'') = [(2m_s/m_{CO}(m_s + m_{CO}))\{E(h\nu) - D_0 - E_s - BJ''(J'' + 1)\}]^{1/2}, \quad (8)$$

where $E(h\nu)$ is the energy of the photon; D_0 is the dissociation energy, taken to be $25\,164 \text{ cm}^{-1}$,¹²³ E_s is 9239 cm^{-1} for the 1D channel and 0 for the 3P channel,³⁴ and $B = 1.9313 \text{ cm}^{-1}$ is the rotational constant in the $v = 0$ level of CO. Since no $CO(v = 1)$ is observed, we will denote $v_{CO}(0, J'')$ simply as $v(J'')$.

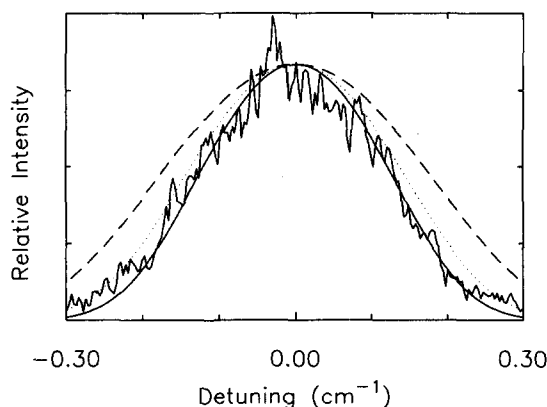


FIG. 6. Doppler profile of the $R(67)$ line in vertical polarization ($\theta' = 90^\circ$) and fits assuming that the CO is produced in coincidence with $S(^1D)$ (solid line) or with $S(^3P)$ (dashed line) and assuming that dissociation takes place from the OCS ground vibrational level. The dotted line is the Doppler profile expected if dissociation of OCS occurs from the $\nu_2 = 1$ level and the CO is produced in coincidence with $S(^1D)$.

For a triatomic parent, spectroscopic selection of $E_{\text{int}}(\text{CO}) = BJ(J+1) + hv[n + (1/2)]$ determines the kinetic energy sharply for each possible sibling atomic state. Thus, the absolute widths of LIF excitation lines allow unambiguous "coincidence"-like determination of sibling atom state for diatomic fragments. This property has been used by Nadler *et al.*¹⁶ to separate the CN rotational distribution from the 266 nm ICN photodissociation into those components produced in coincidence with $I(^2P_{1/2})$ vs $I(^2P_{3/2})$ and by us in Fig. 6, above, to show that all observed CO is produced in coincidence with S(1D).

When the kinetic energy distribution is sharp for each probed fragment state, the angular distributions affect the Doppler line shapes in a particularly simple way. For a linearly polarized photolysis beam with electric vector E_{ph} , the fragment angular distribution is axially symmetric about the polarization direction of the dissociation laser and is given by^{124,125}

$$W(\theta) = (1/4\pi)[1 + \beta P_2(\cos \theta)], \quad (9)$$

where P_2 is the second Legendre polynomial, and θ is the angle between the fragment recoil direction and E_{ph} . The Doppler shifted absorption is shifted from line center (ν_0) by an amount

$$\Delta\nu = \nu_0[1 - (\mathbf{v}(J'') \cdot \mathbf{k}_{\text{pr}}/c)], \quad (10)$$

where c is the speed of light, \mathbf{k}_{pr} gives the direction of propagation of the probe laser, and $\mathbf{v}(J'')$ contains information on the speed, as determined by Eq. (8), and on the angular distribution, as determined by Eq. (9).

Because of the scalar product on the right-hand side of Eq. (10), the Doppler profile will depend on the relative angle of E_{ph} and \mathbf{v} ¹²⁶

$$I(\chi) = \{1 + \beta P_2(\cos \chi) P_2(\cos \theta')\}, \quad (11)$$

where χ is the angle between \mathbf{k}_{pr} and \mathbf{v} , and θ' is the angle between \mathbf{k}_{pr} and E_{ph} . Convolution of Eq. (11) with the laser linewidth and with the transverse distribution of center of mass (c.m.) velocities in the molecular beam then gives the Doppler profile.

The precision of kinetic energy measurements is limited by the linewidth of the VUV light and the c.m.-to-laboratory frame transformation. The molecular beam propagates perpendicular to \mathbf{k}_{pr} , so only the small transverse spread in beam velocities in the dissociated and probed volume contributes to the c.m. transformation. The effective laser linewidth is measured by scanning across the $P(4)$ line of the 2-0 band of CO in a molecular beam of 3% CO in He as shown in Fig. 7(a). [Figure 7(b) will be discussed in Sec. III.] The CO linewidth is fitted well by a Gaussian with a FWHM of 0.21 cm^{-1} . Considering the slight angular divergence of the molecular beam leads to an estimate for the actual laser linewidth of 0.16 cm^{-1} .

The angular distributions of photofragments, as described by the parameter β , can usually be explained by reference to the electronic symmetry of the dissociative excited state and the time scale of dissociation.^{124,127} Perhaps the most striking feature of the CO fragment distribution in this OCS dissociation is the rapid change of β over the relatively

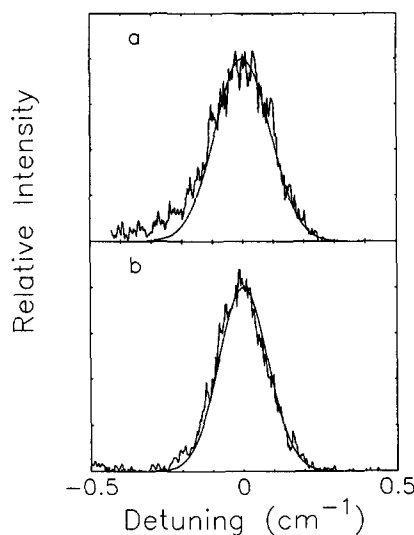


FIG. 7. Doppler profiles for low rotational levels of CO. (a) The $P(4)$ line of the (2-0) band of CO using a molecular beam of 3% CO in He. (b) The $Q(2)$ line of the (2-0) band of CO taken using a molecular beam of 30% OCS in He following photolysis at 222 nm and for the vertical geometrical arrangement ($\theta' = 90^\circ$). In both cases the delay time between the photolysis and probe lasers was 100 ns. The smooth fit in each case is a Gaussian curve with a FWHM of 0.21 cm^{-1} in (a) and 0.19 cm^{-1} in (b).

small range of rotational levels. This change is most evident in the shapes of the Doppler profiles in the first column of Fig. 5, which displays Q -branch transitions for the a geometry characterized by $\theta' = 0$ (which is horizontal polarization in the laboratory). The extraction of quantitative β values from the line shapes shown in Fig. 5 depends on the correct treatment of the vector correlations discussed in the next section, but it is qualitatively evident that the highest J fragments (around 65) are sharply peaked along the dissociation polarization direction, whereas fragments with J values near 50 are more nearly isotropic. How can we understand this variation?

For dipole forbidden electronic transitions that are allowed only by vibronic interactions,^{128,129} such as this $\Delta \leftarrow \Sigma$ transition in OCS, the transition moment can vary dramatically with molecular geometry. For OCS in a linear configuration the transition moment vanishes. As the molecule bends, the Σ state becomes an A' state while the Δ state splits into an A' and an A'' state. It has generally been believed that the 222 nm band of OCS is caused primarily by absorption to the A' and that excitation to the A'' state, which is strictly forbidden in CO_2 and CS_2 , is negligible. However, recent MCD (magnetic circular dichroism) results suggest that the OCS transition has two components.¹³⁰ We therefore suppose that both the A' and A'' states contribute to the absorption.

What fragment anisotropy do we then expect? The $A' \leftarrow A'$ and the $A'' \leftarrow A'$ transitions can each be characterized by a transition moment vector that depends on the bending angle, vanishing in the linear geometry. The $A'' \leftarrow A'$ transition moment will be perpendicular to the triatomic plane, whereas the $A' \leftarrow A'$ transition moment will be in the triato-

mic plane. Prompt dissociation following excitation to the A'' state should give fragment angular distributions with $\beta = -1$, while dissociations from the A' state could potentially give fragments with β anywhere from -1 to 2 , depending on the angle of the transition moment in the plane, relative to the asymptotic recoil direction. If excitation occurs on both the $A' \leftarrow A'$ and the $A'' \leftarrow A'$ transitions and if dissociation on the A' and A'' surfaces gives rise to different rotational distributions, then the anisotropy, characterized by the parameter β , could change dramatically with rotational level. Since it is clear from the experimental data that the angular distributions of the highest CO rotational levels are sharply peaked along the dissociation polarization direction, one of the electronic transitions involved must have its dipole moment aligned nearly along the CS bond. Because the A'' state has its dipole moment perpendicular to the molecular plane and thus perpendicular to the CS bond, it follows that the A' state must be the state responsible for this parallel dissociation channel.

We now formulate a model and compare the Doppler shapes predicted by theory to those observed for the CO photoproduct of OCS dissociation at 222 nm. We suppose that at this wavelength both the A' and A'' states are excited. Since both states are members of a Renner–Teller pair, one may have a bent geometry at the equilibrium OC–S distance for the ground-state parent molecule while the other is nearly linear. We suppose that the A' state is the lower (bent) Renner–Teller component and that the A'' is the upper (linear) component. Both states give rise to rotationally excited CO. Following excitation to the A' state, the OCS molecule will bend as the sulfur atom departs, leading to substantial CO rotation. Dissociative trajectories following excitation to the A'' state would normally lead to little bending and thus negligible CO rotation, but coupling to the A' state during dissociation might still produce substantial rotational excitation. It is known that only Σ vibrational levels can be assigned rigorously to one or the other potential function and that all other vibrational levels of these states will be mixed.¹³¹ We expect therefore that excitation to the A'' (linear) state should give rise to less CO rotation than excitation to the A' (bent) state, but that both excitations can lead to high CO rotational levels. The two peaks in the rotational distribution might be explained by dissociation on the two Renner–Teller surfaces.

What Doppler profiles do we expect for levels in each of the two peaks of the CO rotational distribution? If the peaks at the lower and upper rotational levels arise from excitation to the A'' and A' states, respectively, then the recoil anisotropy should be characterized by low values of β for the lower levels and high values for the upper levels, as is indeed observed. Intermediate levels should be characterized by values of β between -1 and 2 , with Doppler profiles given by Eq. (11).

While the qualitative variation in β is in agreement with the experimental data of Fig. 5, it is clear that the detailed shapes of the Doppler profiles are not in agreement with those of Eq. (11). In particular, Eq. (11) predicts that the profiles for Q vs P or R lines in the same geometry should be the same, whereas the data show dramatic differences. For

example, the $Q(58)$ profile in horizontal polarization ($\theta' = 0$) is markedly different from the $R(58)$ profile for the same geometry. As discussed in a previous publication,¹⁰³ the difference between the Doppler profiles for Q vs P or R lines is due to an angular correlation between the CO recoil velocity vector, \mathbf{v} , and its angular momentum vector, \mathbf{J} . These vectors are required to be perpendicular by conservation of angular momentum: $\mathbf{J}_{\text{OCS}} = \mathbf{J}_s + \mathbf{J} + \mathbf{L}$, where \mathbf{J}_{OCS} is of magnitude ≈ 0 because the parent is prepared in a supersonic expansion, \mathbf{J}_s of magnitude 2 is the angular momentum of the $S(^1D_2)$ atom, \mathbf{J} of magnitude ≈ 59 is the angular momentum of the CO fragment, and \mathbf{L} is the orbital angular momentum. Because $\mathbf{J} \gg \mathbf{J}_s$, it must be true that $\mathbf{J} \approx -\mathbf{L}$, or that the CO rotational vector is antiparallel to the orbital angular momentum. Since the orbital angular momentum must be perpendicular to the recoil velocity \mathbf{v} , we conclude that $\mathbf{J} \perp \mathbf{v}$.

This angular correlation between the rotation and velocity vectors can have a strong influence on the Doppler profile. The detailed line shapes of the Doppler-resolved photofragment spectra depend not only on the kinetic energy and the angular distribution of the fragment velocity \mathbf{v} but also on the angular distribution of the fragment angular momentum vector \mathbf{J} and the correlation between \mathbf{J} and \mathbf{v} . Theory has been developed to describe these effects^{103,132,133} and experimental data have been reported for several molecules, including OCS,¹⁰³ dimethylnitrosamine,¹³⁴ H_2O_2 ,^{135,136} and glyoxal.¹³⁷ The signature of the \mathbf{v}, \mathbf{J} correlation in a parallel fragment transition is a difference in the Doppler line shape for Q branches and P or R branches originating from the same fragment rotational state.

A reasonable first attempt at fitting the Doppler profiles is thus made by assuming that the anisotropy varies with rotational level and that $\mathbf{J} \perp \mathbf{v}$. At first we assumed that \mathbf{J} was cylindrically symmetric about \mathbf{v} . Using either the quantum or classical versions of our own theory^{103,132} or using the equivalent theory developed by Dixon,¹³³ we calculated Doppler profiles for each of the experimentally measured transitions and geometries. While the theories were in agreement with one another and while they qualitatively predicted both the change in shape with rotational level and the difference between the Q - and P - or R -branch lines, the agreement was not quantitative, except at the highest rotational levels, $J > 59$.

The dissociation model proposed above suggests the refinement needed to obtain quantitative agreement with the data. For excitation to the A'' state, the parent molecule's transition dipole moment, μ_p , will be perpendicular to \mathbf{v} , and from conservation of angular momentum we have concluded that $\mathbf{J} \perp \mathbf{v}$ for dissociation from either state. But what is the relationship between \mathbf{J} and μ_p ? In the previously described calculations we assumed that \mathbf{J} was cylindrically symmetric about \mathbf{v} , as would be appropriate when μ_p is parallel to \mathbf{v} . But when both μ_p and \mathbf{J} are perpendicular to \mathbf{v} , the assumption of cylindrical symmetry may no longer be valid. In fact, for excitation to the A'' state the transition moment is perpendicular to the plane of the bent OCS, and since \mathbf{J} must also be perpendicular to the molecular plane, we conclude that for dissociations rapid enough so that the plane does not rotate

between excitation and dissociation, \mathbf{J} must be parallel to μ_p . The dipole μ_p will always tend to be aligned along the electric vector of the dissociating light, so for rapid dissociations \mathbf{J} will also tend to be aligned in this direction; i.e., it will no longer be cylindrically symmetric about \mathbf{v} .

Doppler profiles were then calculated on the assumption that a fraction of the dissociative events f takes place on the A' surface with $\beta = 2$, $\mathbf{J} \perp \mathbf{v}$, and \mathbf{J} cylindrically symmetric about \mathbf{v} , while the remaining fraction $1-f$ takes place on the A'' surface with $\beta = -1$, $\mathbf{J} \perp \mathbf{v}$, and $\mathbf{J} \parallel \mu_p$. Bipolar moments of the distribution¹³⁶ can be calculated as a linear interpolation between the set $\{\beta_0^2(20), \beta_0^2(02), \beta_0^0(22), \beta_0^2(22), \beta_0^2(42), \beta_0^2(24), \beta_0^0(44), \beta_0^2(44), \beta_0^2(64)\}$, $= \{1, -0.5, -0.5, 0.5, -0.5, 0.375, 0.375, -0.375, 0.375\}$ for $f=1$ and $\{-0.5, 1.0, -0.5, 0.5, 0.375, -0.5, 0.375, -0.375, -0.312\}$ for $f=0$. Because the Doppler profiles are linearly proportional to the bipolar moments, the resulting Doppler profile for any intermediate value of f can be described simply as a linear combination of the profiles expected for the two limiting cases. The smooth lines through the data in Fig. 5 are the Doppler profiles calculated in this manner with the *single adjustable parameter* f and convoluted with the laser linewidth. Values of the interpolation parameter f are provided in Table I, which also lists the bipolar moments calculated from this parameter for each set of data. The error limits for the parameter f , estimated from the quality of the fits to the data, vary smoothly from ± 0.02 for rotational levels near $J = 50$ to ± 0.05 at $J = 68$.

Several other assumptions concerning the angular momentum distribution were tested and found not to be consistent with the data. In particular, the assumption that $\mathbf{J} \perp \mu_p$ for the component with $\beta = -1$ produced profiles which deviated significantly from those observed. This assumption would model pure absorption to the A' component of the ${}^1\Delta$ state, with a transition moment direction which changed with the degree of bending. The quantitative agreement shown in Fig. 5 was obtained for all levels with $J > 50$ and lends strong support to the dissociation model proposed above where absorption takes place to both the A' and A'' components.

For levels with $J \leq 50$ the agreement was not perfect. The signal levels fall sharply with lower values of J , and all Doppler profiles deviated slightly from those calculated. The deviations were the same for all lines and all geometries: too much intensity was observed in the center of the Doppler profile. Since such a deviation cannot be accounted for by any adjustment of the bipolar moments, the source of the discrepancy for $J \leq 50$ must be sought elsewhere. One possible explanation for this slight deviation in the five levels observed is that dissociation of OCS clusters may produce some rotationally excited CO with low translational recoil, thus adding a small amount of intensity to the Doppler profile centers. Such an effect would be most evident when the signal levels from the monomer dissociation were small.

The Doppler profiles of $S({}^1D)$ provide an independent check on the interpretation of the OCS photodissociation presented above and based on the CO internal energy distribution and the CO Doppler profiles. A trial fit to the $S({}^1D)$ line shapes can be constructed as a composite of profiles each

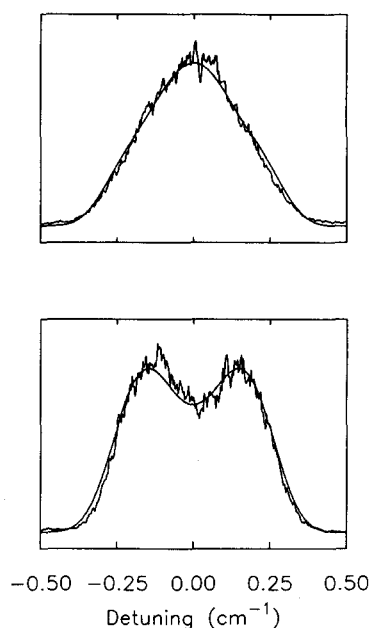


FIG. 8. Doppler profiles of the $S({}^1D)$ line in vertical (top, $\theta' = 90$) and horizontal (bottom, $\theta' = 0$) polarization. The smooth lines are composite profiles predicted assuming that each CO rotational level has a sibling $S({}^1D)$ atom with a speed determined by energy and momentum conservation, an anisotropy parameter equal to that of the sibling CO, and a weight proportional to the CO population. The good agreement provides further confirmation of the dissociation model.

given by Eq. (13). We assume that each CO rotational level has a sibling $S({}^1D)$ atom with a speed determined by energy and momentum conservation, an anisotropy parameter equal to that of the sibling CO [from Table I, $2\beta_0^2(20)$], and a weight proportional to the CO population [from Fig. 4(c)]. These simulated $S({}^1D)$ line shapes are qualitatively in good agreement with experimental measurements, but are slightly wider than the observed lines. The experimentally missing high-speed sulfur atoms are the ones that correspond to the low J tail of the CO distribution in Fig. 4(c). We have already argued that at $J \leq 50$ the CO Doppler profiles have a slower component which we attribute to a cluster dissociation channel. The $S({}^1D)$ lines are also consistent with this interpretation. Shown in Fig. 8 are $S({}^1D)$ Doppler profiles in two polarizations and the composite simulations, assuming that CO with $J < 48$ is predominately from a cluster channel and is not accompanied by $S({}^1D)$ with a speed appropriate for monomer dissociation. We note briefly that an attempt to fit the $S({}^1D)$ lines with a single β and the speed distribution corresponding to the CO rotational distribution fails to give a satisfactory fit for any value of β .

We conclude that the quantitative agreement between the Doppler profiles expected from our model and those actually observed lends strong support to the model. The model also explains the bimodal rotational distribution observed for dissociation at 222 nm. That the distribution is no longer bimodal for dissociation at 248 and 235 nm might be explained by assuming that the lower photon energy can no longer access the upper A'' state or that the rotational distri-

contributions from the two states are much more similar for lower photolysis energies. If the former is the explanation for the single peaks in the rotational distributions at the longer wavelengths, then all rotational levels in these distributions should be characterized by transitions with $\beta \approx 2$, J_{1v} , and J cylindrically symmetric about v , while if the latter is the explanation it would be expected that β should still vary substantially with J . These experiments remain to be performed.

We now consider two consequences of this model. One clear conclusion is that dissociation is prompt; i.e. that there is little or no rotation of the parent OCS molecule between excitation and dissociation. While it is not particularly surprising that a bent OCS molecule does not have time to rotate about its b or c axes, it is at first surprising that it does not rotate about its a axis on the time scale of dissociation. Experimental evidence for the absence of such rotation is provided by the observation that, for dissociation via the A'' surface, the Doppler profiles are fit only if it is assumed that J and μ_p are parallel; i.e., that J will tend to be aligned with the electric vector of the dissociating light. Rotation about the a axis on a time scale rapid with respect to dissociation would destroy such alignment. Such rotation might at first be thought to be rapid since one unit of vibrational angular momentum in the linear ground state gives a frequency corresponding to the bending quantum of 520 cm^{-1} , or a rotation time of 64 fs. However, the moment of inertia about the a axis is an extremely strong function of bending angle; the A constant decreases to 15 cm^{-1} or the rotation time to 2 ps for a bending angle of only 20° . The rotational distributions have already made it quite clear that the OCS molecule bends substantially during dissociation. As soon as this bending starts to occur, molecular rotation about the a axis is dramatically slowed.

A further question which is raised by the model is why the transition moment for the A' state lies nearly along the CS bond. For an electronically forbidden transition, the alignment of the transition dipole in the OCS plane will depend on the vibronic coupling which gives the transition oscillator strength. Previous inferences about vibronic coupling and transition moments in the $\Delta \leftarrow \Sigma$ transition of OCS have been reported, based on the temperature dependence of integrated band intensities and average transition frequencies.^{94,138,139} Good fits to the temperature dependence of the absorption intensities were obtained assuming a transition moment linear in the bending coordinate, and higher order couplings were therefore neglected. The first order vibronic coupling of a Δ electronic state with a bend (of π symmetry) would allow intensity borrowing from the nearby Π electronic state. By this mechanism alone, the transition moment should be perpendicular to the triatomic axis and we should see all fragments characterized by $\beta = -1$, contrary to our observations. In order to see fragments with positive β , the Δ state must borrow intensity from Σ states, which requires two antisymmetric vibrations, i.e., quadratic vibronic coupling, in the Herzberg–Teller language.¹²⁸

A resolution to this apparent discrepancy is suggested by considering the analogous ${}^1\Delta_u \leftarrow {}^1\Sigma_g^+$ transition in CO_2 . The transition moments have been calculated by Julienne *et*

*al.*¹⁴⁰ in order to estimate temperature-dependent absorption cross sections. In this higher symmetry molecule, the transition is vibronically forbidden in first order,¹⁴¹ and one sees that the leading dependence of the transition moment on the bending angle is quadratic at small angles. Significantly, however, the *ab initio* calculations show that the transition moment stops increasing quadratically at bending angles less than the average zero-point bend and could be fit reasonably well by a straight line throughout most of the bending angles accessed by the first few vibrational levels. The rapid deviation of the actual transition moment from the truncated power series expansion in the bending angle is not surprising due to the large geometry change in the excited state.¹⁴¹ The same effect might be expected in OCS, except that the linear vibronic coupling is not symmetry forbidden. We are led to conclude that, while the ${}^1\Delta \leftarrow {}^1\Sigma^+$ transition moment increases in length approximately linearly with the bending coordinate, the rate of increase is not necessarily related to the strength of the linear vibronic coupling, and the direction of the transition moment need not be in the direction characteristic of the pure linear vibronic coupling.

We close this section by considering another possible state of OCS which might contribute to the dissociation at 222 nm. The observed Doppler profiles are consistent with contributions to the dissociation from both an A'' and an A' state; we have assumed these to be the two Renner–Teller components split from the linear ${}^1\Delta$ state. Another possibility exists for the A'' component, namely a ${}^1\Sigma^-$ state predicted to lie somewhat lower than the ${}^1\Delta$ state in energy but never before observed. Were the ${}^1\Sigma^-$ state to actually have a bent geometry, its symmetry would be reduced to A'' . The measurements we have made to date cannot distinguish whether the A'' component to the dissociation is due to the upper Renner–Teller component of the ${}^1\Delta$ state or to the ${}^1\Sigma^-$ state. However, measurements of CO Doppler profiles for dissociation at another wavelength might suggest a choice, since the ratio of A' to A'' excitation will be different under these alternate assumptions. At lower dissociation energy, we would expect less A'' character if such character arises from the upper Renner–Teller component of the ${}^1\Delta$ state, whereas we would expect more A'' character if such character arises from the ${}^1\Sigma^-$ state. These experiments remain to be performed.

C. Dissociation of OCS clusters

1. CO fragment from clusters

As discussed in a previous publication,¹⁰² the intensity of CO LIF near the (2,0) bandhead depends dramatically on the partial pressure of OCS in the source, an observation which implies that the parent compounds responsible for these CO products are van der Waals clusters. Detailed measurements show that the intensity of the bandhead lines varies roughly as the square of the partial OCS backing pressure.¹⁴² The CO rotational distribution in this bandhead region can be described adequately by a rotational temperature of 50 K. Time-resolved studies show that the cold CO product is formed promptly, within 50 ns of photolysis. In Fig. 7, the Doppler profiles for low J CO lines are shown for

(a) CO in a supersonic jet of 3% CO in He, and (b) the cold CO photoproduct resulting from 222 nm photolysis of a beam containing 30% OCS in He. In both cases, the Doppler profiles are essentially Gaussian line shapes with widths (FWHM) of 0.21 cm^{-1} for the 3% CO in He beam and 0.19 cm^{-1} for the cold CO product.

Under the expansion conditions used to observe the cold CO photoproduct, separate experiments using a quadrupole mass spectrometer showed that the supersonic beam contained significant quantities of large clusters, with mass peaks observed up to $(\text{OCS})_{10}^+$. The signals for the larger ions $(\text{OCS})_6^+$ through $(\text{OCS})_8^+$ displayed a dependence on OCS partial pressure similar to that observed for the cold CO product signal.

2. S_2 products from clusters

Both $\text{S}_2(X^3\Sigma_g^-)$ and $\text{S}_2(a^1\Delta_g)$ were also produced following 222 nm photolysis of OCS under expansion conditions similar to those used when the rotationally cold CO was observed. The S_2 products were detected by LIF using the transitions $\text{S}_2(B^3\Sigma_u^-) \leftarrow \text{S}_2(X^3\Sigma_g^-)$ (6,0) near 293 nm and $\text{S}_2(f^1\Delta_u) \leftarrow \text{S}_2(a^1\Delta_g)$ (5,0) near 264 nm. Just as in the case of the rotationally cold CO, the appearance time of the S_2 product was prompt, as shown in Figs. 9(a) and 9(b). Figure 9(c) displays the temporal appearance of the $\text{S}_2(X^3\Sigma_g^-)$ LIF signal following the bimolecular reaction of $\text{S}(^1D) + \text{OCS}$ in a slow flow of OCS at a pressure of 200 mTorr. This signal was measured under the same excitation and viewing geometry as used for the molecular beam signals in Figs. 9(a) and 9(b). The bimolecular reaction is clearly much slower. The rate constant for the $\text{S}_2(X^3\Sigma_g^-)$ appearance in Fig. 9(c) is $1.4 \times 10^{-10} \text{ cm}^3 \text{ molecule}^{-1} \text{ s}^{-1}$, in good agreement with the literature value,¹⁴³ obtained from the decay of the $\text{S}(^1D)$ signal in the presence of OCS.

The rotational distribution of the $\text{S}_2(X^3\Sigma_g^-)$ product of cluster dissociation was measured using the (6,0) band and can be described approximately by a Boltzmann distribution with a temperature of $100 \pm 15 \text{ K}$.¹⁴² Molecular constants and Hönl–London factors were taken from the literature.¹⁴⁴ Although the contour of the intense part of the measured spectrum is given by a temperature of 100 K, the observed population of higher rotational lines is higher than that predicted by such a distribution. By contrast, the S_2 rotational distribution that results from the bimolecular reaction of $\text{S}(^1D)$ with OCS is Boltzmann with a temperature of 150 K.¹¹⁶ As in the case of the reaction, no population was observed in $v = 1$.

The rotational distribution for the $\text{S}_2(a^1\Delta_g, v = 1)$ level was calculated using the LIF spectrum of the (5–1) band. The distribution peaks at approximately $J = 65$, in rough agreement with the distribution found from the bimolecular reaction.¹¹⁶ As discussed elsewhere, unfavorable Franck–Condon factors make it very difficult to study the $v = 0$ level.¹¹⁶

3. Discussion

Arguments supporting an identification of the rotationally cold CO with the product of photofragmentation of

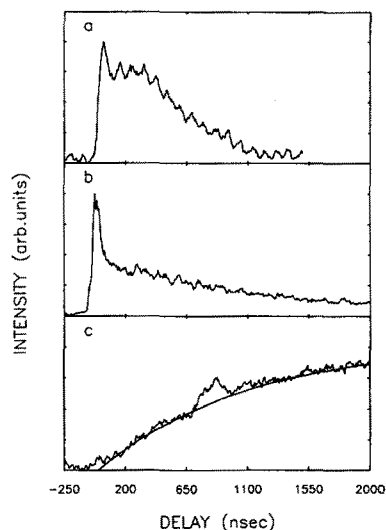


FIG. 9. The dependence of the LIF signal of S_2 products on the delay time between the probe and photolysis lasers. The photolysis wavelength is 222 nm. (a) $\text{S}_2(^3\Sigma_g^-)$ produced following photolysis of a beam of 30% OCS in He. (b) $\text{S}_2(^1\Delta_g)$ produced following photolysis of a beam of 30% OCS in He. (c) $\text{S}_2(^3\Sigma_g^-)$ produced following photolysis of 200 mTorr of flowing OCS. The fit is $I(t) = 1 - \exp(-k[\text{OCS}]t)$, where $k = 1.4 \times 10^{-10} \text{ cm}^3 \text{ molecule}^{-1} \text{ s}^{-1}$ and $[\text{OCS}]$ is the density in molecules cm^{-3} .

OCS clusters have been presented briefly by us in a previous publication.¹⁰² Strong evidence that the portion of the CO distribution with a 50 K rotational temperature cannot be a result of monomer photolysis comes from the appearance time of the cold CO signal and from the dependence of its intensity on the OCS partial pressure in the source. The cold CO is formed promptly (within our 50 ns time resolution) and has a yield that depends on the square of the OCS partial pressure. In contrast, the yield of the rotationally excited CO photoproduct has a nearly linear dependence on OCS pressure. This difference in behavior indicates that the cold CO product arises either from secondary collisions in the beam or from collisionless photolysis of OCS clusters. Secondary collisions can easily be ruled out because of the prompt appearance of the cold CO product. Any collisional mechanism, such as rotational relaxation of the CO photoproduct or a bimolecular reaction between $\text{S}(^1D)$ and OCS, would require an extremely large cross section, on the order of 150 or 600 \AA^2 , respectively, to form cold CO within 50 ns. Such large cross sections are physically unreasonable, especially since the cross sections for these processes are known to be small. Rotational relaxation of high rotational levels of CO is slower than gas kinetic,¹¹⁰ while the cross section for reaction has been measured to be only 15 \AA^2 .¹¹⁶

The Doppler profiles of absorption lines for the cold CO product molecules provide a further key to the mechanism of their formation. In addition to being rotationally cold, we find that these products are also translationally cold. The VUV laser used to record the line profiles has a linewidth of 0.16 cm^{-1} (FWHM). For a free jet of 3% CO in He, the measured line profile has a width of 0.21 cm^{-1} , which is a result of the laser linewidth and a Doppler broadening of

0.14 cm^{-1} caused by the divergence of the molecular beam and the large viewing zone of our light collection optics. The 0.14 cm^{-1} width corresponds to the sampling by our optics of a 10° half angle beam divergence, a reasonable value for a free-jet expansion. For the spectral lines corresponding to the cold CO photoproduct, the measured line profile was essentially Gaussian with a width of 0.19 cm^{-1} (FWHM), as shown in Fig. 7(b). This linewidth results from a convolution of three factors: the 0.16 cm^{-1} laser linewidth, the divergence of the molecular beam, and the Doppler width caused by any translational excitation in the rotationally cold CO product. Since the molecular beam used in this case was 30% OCS in He, the beam velocity is about a factor of 2 less than that obtained for the 3% mixture of CO in He (8×10^4 vs $1.6 \times 10^5 \text{ cm/s}$). The effective divergence is also smaller in the case of the CO from dissociation of OCS, because the intersection of the molecular jet with the crossed laser beams defines a smaller volume than does the intersection of the jet with the probe laser alone. Based on the lower velocity and smaller volume, a 0.07 cm^{-1} width from the beam divergence would be expected. In order for the three contributing factors to result in a linewidth of 0.19 cm^{-1} , the line broadening caused by the translational energy of the CO must be no more than 0.07 cm^{-1} . This width corresponds to a translational temperature of 60 K, which is about the same as the rotational temperature of the cold CO photoproduct.

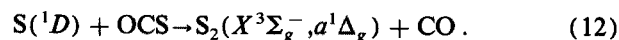
The finding that the rotationally cold CO is also translationally cold provides further evidence that this CO product is formed neither as a result of bimolecular collisions nor as a result of the primary photodissociation. As has already been discussed, the high rotational levels of CO are formed with appreciable translational energy. Rotational relaxation of these levels by collisions with He in the beam could not simultaneously produce a lower translational energy. Nor can the cold CO result from the bimolecular reaction $\text{OCS} + \text{S}(^1D) \rightarrow \text{S}_2 + \text{CO}$. Based on previous studies¹¹⁶ of the energy partitioning into the S_2 product of this reaction, a cold CO product would carry about $13\,000 \text{ cm}^{-1}$ of translational energy, requiring a Doppler width of at least 0.6 cm^{-1} . Similarly, a rotationally cold CO product from primary dissociation of the OCS monomer would require a Doppler width of 0.5 cm^{-1} .

Mass spectral analysis of the pulsed beam indicates that there is extensive OCS clustering under the expansion conditions used to observe the cold CO photoproduct. As is well known, electron impact ionization results in fragmentation of weakly bound molecular clusters,¹⁴⁵ and thus the observation of mass 480 in the mass spectrum of the OCS beam indicates only that $(\text{OCS})_n$ clusters with $n \geq 8$ are present; the mass spectral intensities cannot be used to derive a quantitative cluster size distribution. However, from the observed dependence of the various mass signals on OCS partial pressure, it can be argued that only the larger OCS clusters ($n \geq 6$) have a concentration that depends on the square of the OCS partial pressure in the source. This argument, in turn, implies that the cold CO product is formed from photolysis of large OCS clusters.

If the cold CO is produced predominantly from large OCS clusters, then its Doppler profile and rotational tem-

perature can be used to suggest a mechanism for the product formation. A prompt CO photoproduct can only result from either OCS photolysis or the reaction of an $\text{S}(^1D)$ photoproduct with an OCS molecule *in the same cluster*. Since either CO product would be translationally excited, especially at low J , the rotationally cold photoproduct observed by us must result from collisional relaxation of the CO before it escapes from the cluster, a process that will result in both translational and rotational cooling. Since either OCS photolysis or $\text{S} + \text{OCS} \rightarrow \text{CO} + \text{S}_2$ will impart a considerable amount of energy to the CO product, the cluster will have to accommodate substantial energy in order to cool the nascent CO to 60 K. A large cluster with many vibrational modes must be required since the van der Waals bond energy of OCS in the cluster is only on the order of 250 cm^{-1} .¹⁴⁶ We conclude that the cold CO photoproduct is the result of photolysis of OCS molecules contained in large OCS clusters (clusters with more than six OCS molecules) and that the CO photoproduct is rotationally and translationally relaxed and it escapes from the cluster.

The prompt S_2 photoproduct is also produced by photolysis of OCS clusters, most likely as the result of a reaction within the cluster of a photolytically generated $\text{S}(^1D)$ atom with another OCS molecule:



As can be seen in Figs. 9(a) and 9(b), the signals from both $\text{S}_2(^3\Sigma_g^-)$ and $\text{S}_2(^1\Delta_g)$ appear promptly following the photolysis pulse. Figure 9(c) shows the time evolution expected if the S_2 product resulted from secondary collisions. The growth time for the S_2 signal is microseconds, even at a pressure of OCS that is significantly higher than that in the beam.

The observation of a reaction within a van der Waals cluster is not surprising, since the nascent $\text{S}(^1D)$ atom will have enough translation energy to overcome any barrier to reaction and since the probability of a collision with another OCS molecule in the cluster is high. This technique of initiating a reaction in a van der Waals cluster has recently been used by Wittig and co-workers^{104,147,148} to study the steric dependence of the reaction $\text{H} + \text{CO}_2 \rightarrow \text{OH} + \text{CO}$. The HBr moiety in $\text{CO}_2 \cdot \text{HBr}$ complexes was photolyzed at 193 nm, and the H atom produced in the dissociation reacted with the CO_2 in the complex, resulting in a prompt OH product which was detected by laser-induced fluorescence. In similar experiments, pulsed laser excitation of Hg atoms in $\text{Hg} \cdot \text{H}_2$ clusters was used to initiate the reaction $\text{Hg}(^3P) + \text{H}_2 \rightarrow \text{HgH} + \text{H}$.¹⁰⁷

The S_2 signal observed in our work did not show as strong a dependence on OCS partial pressure as did the cold CO product. In fact, an S_2 signal was observed even at the lowest OCS concentration used, where the cold CO signal had essentially disappeared. A pressure dependence similar to that for the S_2 signals was also observed for the lower cluster ion signals in the mass spectrometer experiments, implying that the smaller clusters are mostly responsible for the S_2 observed. The internal energy of the S_2 products also suggests that most of the observed S_2 product arises from smaller clusters. For both the $\text{S}_2(^3\Sigma_g^-)$ and $\text{S}_2(^1\Delta_g)$ products, the rotational distributions observed under the cluster

conditions were similar to those observed in the bimolecular reaction in the gas phase.¹¹⁶ This behavior is similar to the $\text{H} + \text{CO}_2$ reaction occurring in $\text{HBr}\cdot\text{CO}_2$ clusters,^{104,147,148} where the rotational distribution of the OH product was found to be similar to the gas-phase result, but with a little less energy in rotation.

The apparent difference in behavior between large and small clusters is quite reasonable. We expect the distribution of clusters in our beam to favor smaller clusters under the beam conditions used in these experiments. Since the probability of an internal $\text{S}(^1D) + \text{OCS}$ reaction is high, even in small clusters, the observed S_2 product will be dominated by reactions within the small clusters and will thus look similar to the bimolecular S_2 product.

The cold CO product, on the other hand, can only be the result of extensive rotational and translation relaxation of the nascent CO within a single cluster. As smaller clusters cannot accommodate this amount of energy, any cold CO observed will be the result of large cluster photolysis. In fact, there will be a wide distribution of $\text{CO}(v=0, J)$ products from smaller cluster photolysis, where the J is intermediate between $J=0$ and $J=55$, the peak of the monomer distribution. There is some indication of intermediate rotational levels in the Doppler profiles observed for the $\text{CO}(J < 50)$ photoproduct, where there is evidence of a lower velocity of CO product contributing to the Doppler line shape. Such a product would be the result of partial relaxation of a CO photoproduct in a small cluster, where one might expect an effective relaxation of translation, but less effective rotational relaxation.

The dramatic change that occurs at the bandhead region of the CO product spectrum results from the fact that the CO product from very large clusters "piles up" at low J because of the low internal temperature of the clusters. Smaller clusters produce a broad range of $\text{CO}(J)$ products, and the resulting LIF signal is spread over many lines so that these CO molecules do not show up as dramatically as those from the large clusters.

IV. CONCLUSION

An important and general conclusion from the results and discussion presented above is that measurement of Doppler profiles of photofragments can provide much more information about photodissociative events than has previously been realized. For a triatomic parent compound, this information can be summarized as follows. The widths of the profiles are constrained by conservation of energy and by the internal energy of the probed fragment. The distribution of widths is thus directly related to the distribution of energies in the unprobed fragment. The shapes of the Doppler profiles are determined by the correlations between three vector quantities: μ_p , the transition dipole moment of the parent triatomic; \mathbf{J} , the product angular momentum; and \mathbf{v} , the recoil velocity. In many cases, the shapes allow an unambiguous determination of the vector correlations. For large values of \mathbf{J} and for dissociation of a triatomic parent compound from very low rotational levels, conservation of angular momentum will restrict \mathbf{J} to be nearly perpendicular to \mathbf{v} . This correlation will persist no matter what the time scale of dis-

sociation. The distribution of \mathbf{v} with respect to μ_p , and hence (for prompt dissociations) with respect to the electric vector of the dissociating light, can be used to determine the direction of the transition dipole in the molecular frame. For electronically forbidden transitions, this direction will depend strongly on vibronic coupling. In the case when the transition dipole moment has a component orthogonal to the recoil velocity, then (for prompt dissociations) the alignment resulting from the angular correlation between \mathbf{J} and μ_p can be used to determine whether μ_p lies in or out of the molecular plane.

Application of these techniques to the $\Delta \leftarrow \Sigma$ dissociation of OCS has shown the following model to be consistent with the experimental results. Photolysis at 222 nm excites both the A'' and A' Renner-Teller components of the $^1\Delta$ state. The lower of these components (A') has a bent geometry at the OC-S ground-state internuclear separation. Following excitation to either component, bending in the excited state during dissociation leads to extensive rotational excitation of the CO fragment, but in the case of excitation to the linear A'' component the bending arises from vibrational coupling to the A' component so that a somewhat colder distribution is observed than from direct excitation of the A' state. Two peaks are thus observed in the rotational distribution. Because the CO bond is relatively unaffected by the dissociation, CO is produced primarily in $v=0$. The moment for the A' transition is nearly parallel to the C-S bond, so that dissociation on this surface occurs with μ_p parallel to \mathbf{v} ($\beta=2$). The moment for the A'' transition is perpendicular to the plane of the OCS molecule, so that dissociation on this surface occurs with μ_p perpendicular to \mathbf{v} ($\beta=-1$) and with μ_p parallel to \mathbf{J} . In both cases, conservation of angular momentum restricts \mathbf{J} to be perpendicular to \mathbf{v} . All dissociative events produce $\text{S}(^1D)$; an upper limit on the $\text{S}(^3P)$ channel is 2%.

The product distribution from dissociation of OCS clusters depends on the size of the cluster. Vibrationally, rotationally, and translationally cold CO is produced as a result of photolysis of large clusters: $(\text{OCS})_n$ with $n \geq 6$. Photolysis of smaller clusters is responsible for the S_2 product, which arises when dissociation of one OCS molecule in the cluster produces a sulfur atom that reacts with another OCS molecule in the same cluster. The CO from photolysis of these small clusters, either produced in direct dissociation of one of the OCS molecules or as a product of the $\text{S} + \text{OCS}$ reaction, is partially relaxed rotationally and greatly cooled translationally as it leaves the cluster. Portions of this relaxed distribution are observed at levels between $J=45$ and $J=50$, where the Doppler profiles show small amounts of CO with low velocity.

ACKNOWLEDGMENTS

Partial support for this work was provided by the Air Force Office of Scientific Research (AFOSR-86-0017), by the National Science Foundation (CHE-8314146, CHE-8617062), and by the Environmental Protection Agency (CR-811010-01-0). J.W.H. would like to acknowledge the support of NSERC (Canada). P.L.H. would like to acknowledge the support of the John Simon Guggenheim

Foundation. We would also like to thank Professor A. C. Albrecht and Dr. E. Goldfield for valuable discussions and C. E. Strauss and G. C. McBane for help in the experimental work leading to the results presented in Fig. 2.

- ¹G. G. Balint-Kurti and M. Shapiro, *Chem. Phys.* **61**, 137 (1981).
- ²R. J. Donovan and J. Konstantatos, *J. Photochem.* **1**, 75 (1972).
- ³K. E. Holdy, L. C. Klotz, and K. R. Wilson, *J. Chem. Phys.* **52**, 4588 (1970).
- ⁴J. H. Ling and K. R. Wilson, *J. Chem. Phys.* **63**, 101, (1975).
- ⁵M. J. Sabety-Dzvonik, and R. J. Cody, *J. Chem. Phys.* **66**, 125 (1977).
- ⁶A. P. Baronavski and J. R. McDonald, *Chem. Phys. Lett.* **45**, 172 (1977).
- ⁷J. A. Beswick and J. Jortner, *J. Chem. Phys.* **24**, 1 (1977).
- ⁸U. Halavee and M. O, *Chem. Phys.* **21**, 105 (1977).
- ⁹M. D. Morse, K. F. Freed, and Y. B. Band, *J. Chem. Phys.* **70**, 3620 (1979).
- ¹⁰S. T. Amimoto, J. R. Wiesenfeld, and R. H. Young, *Chem. Phys. Lett.* **65**, 402 (1979).
- ¹¹W. M. Pitts and A. P. Baronavski, *Chem. Phys. Lett.* **71**, 395 (1980).
- ¹²A. P. Baronavski, *Chem. Phys.* **66**, 217 (1982).
- ¹³W. Kreiger, J. Häger, and J. Pfab, *Chem. Phys. Lett.* **85**, 69 (1982).
- ¹⁴W. H. Fisher, T. Carrington, S. V. Filseth, C. M. Sadowski, and C. H. Dugan, *Chem. Phys.* **82**, 443 (1983).
- ¹⁵I. Nadler, H. Reisler, and C. Wittig, *Chem. Phys. Lett.* **103**, 451 (1984).
- ¹⁶I. Nadler, D. Mahgerefteh, H. Reisler, and C. Wittig, *J. Chem. Phys.* **82**, 3885 (1985).
- ¹⁷B. A. Waite, H. Helvajian, B. I. Dunlap, and A. P. Baronavski, *Chem. Phys. Lett.* **111**, 544 (1984).
- ¹⁸W. J. Marinelli, N. Sivakumar, and P. L. Houston, *J. Phys. Chem.* **88**, 6685 (1984).
- ¹⁹E. M. Goldfield, P. L. Houston, and G. S. Ezra, *J. Chem. Phys.* **84**, 3120 (1986).
- ²⁰G. E. Hall, N. Sivakumar, and P. L. Houston, *J. Chem. Phys.* **84**, 2120 (1986).
- ²¹J. V. V. Kasper and G. C. Pimentel, *Appl. Phys. Lett.* **5**, 231 (1964).
- ²²S. J. Riley and K. R. Wilson, *Discuss. Faraday Soc.* **53**, 132 (1972).
- ²³M. J. Dzvonik and S. C. Yang, *Rev. Sci. Inst.* **45**, 750 (1974).
- ²⁴S. L. Baughcum and S. R. Leone, *J. Chem. Phys.* **72**, 6531 (1980).
- ²⁵R. K. Sparks, K. Shobatake, L. R. Carlson, and Y. T. Lee, *J. Chem. Phys.* **75**, 3838 (1981).
- ²⁶H. W. Hermann and S. R. Leone, *J. Chem. Phys.* **76**, 4759 (1982).
- ²⁷G. N. A. van Veen, T. Baller, A. E. de Vries, and N. J. A. van Veen, *Chem. Phys.* **87**, 405 (1984).
- ²⁸M. D. Barry and P. A. Gorry, *Mol. Phys.* **52**, 461 (1984).
- ²⁹M. Shapiro and R. Bersohn, *J. Chem. Phys.* **73**, 3810 (1980).
- ³⁰A. Gedanken and M. D. Rowe, *Chem. Phys. Lett.* **34**, 39 (1975).
- ³¹S. Lee and E. J. Heller, *J. Chem. Phys.* **76**, 4766 (1982).
- ³²S. K. Gray and M. S. Child, *Mol. Phys.* **51**, 189 (1984).
- ³³M. Shapiro, *J. Phys. Chem.* **90**, 3644 (1986).
- ³⁴P. Andresen, G. S. Ondrey, B. Titze, and E. W. Rothe, *J. Chem. Phys.* **80**, 2548 (1984).
- ³⁵P. Andresen, G. S. Ondrey, and B. Titze, *Phys. Rev. Lett.* **50**, 486 (1983).
- ³⁶P. Andresen and E. W. Rothe, *Chem. Phys. Lett.* **86**, 270 (1982).
- ³⁷P. Andresen and E. W. Rothe, *J. Chem. Phys.* **78**, 989 (1983).
- ³⁸M. P. Docker, A. Hodgson, and J. P. Simons, *Mol. Phys.* **57**, 129 (1986).
- ³⁹A. Hodgson, J. P. Simons, M. N. R. Ashfold, J. M. Bayley and R. N. Dixon, *Chem. Phys. Lett.* **107**, 1 (1984).
- ⁴⁰A. Hodgson, J. P. Simons, M. N. R. Ashfold, J. M. Bayley, and R. N. Dixon, *Mol. Phys.* **54**, 351 (1985).
- ⁴¹J. P. Simons and A. J. Smith, *Chem. Phys. Lett.* **97**, 1 (1983).
- ⁴²J. P. Simons, A. J. Smith, and R. N. Dixon, *J. Chem. Soc. Faraday Trans. II* **80**, 1489 (1984).
- ⁴³P. L. Houston and C. B. Moore, *J. Chem. Phys.* **65**, 757 (1976).
- ⁴⁴C.-K. Cheng, P. Ho, C. B. Moore, and M. B. Zughul, *J. Phys. Chem.* **88**, 286 (1984).
- ⁴⁵M. Pealat, D. Debarre, J. -M. Marie, J. -P. E. Taran, A. Tramer, and C. B. Moore, *Chem. Phys. Lett.* **98**, 299 (1983).
- ⁴⁶P. Ho, D. J. Bamford, R. J. Buss, Y. T. Lee, and C. B. Moore, *J. Chem. Phys.* **76**, 3630 (1982).
- ⁴⁷P. Ho and A. V. Smith, *Chem. Phys. Lett.* **90**, 407 (1982).
- ⁴⁸S. K. Gray, W. H. Miller, Y. Yamaguchi, and H. F. Schaefer III, *J. Am. Chem. Soc.* **103**, 1900 (1981).
- ⁴⁹J. D. Goddard and H. F. Schaefer III, *J. Chem. Phys.* **70**, 5117 (1979).
- ⁵⁰W. H. Miller, *J. Am. Chem. Soc.* **101**, 6810 (1979).
- ⁵¹B. A. Waite, S. K. Gray, and W. H. Miller, *J. Chem. Phys.* **78**, 259 (1983).
- ⁵²W. H. Miller, *J. Am. Chem. Soc.* **105**, 216 (1983).
- ⁵³J. C. Weishaar and C. B. Moore, *J. Chem. Phys.* **70**, 5135 (1979); **72**, 2875 (1980); **72**, 5415 (1980).
- ⁵⁴D. J. Bamford, S. V. Filseth, M. F. Foltz, J. W. Hepburn, and C. B. Moore, *J. Chem. Phys.* **82**, 3032 (1985).
- ⁵⁵D. Debarre, M. Lefebvre, M. Péalat, J. -P. E. Taran, D. J. Bamford, and C. B. Moore, *J. Chem. Phys.* **83**, 4476 (1985).
- ⁵⁶J. W. Rabalais, J. M. Mac Donald, V. Scherr, and S. P. McGlynn, *Chem. Rev.* **71**, 73 (1971).
- ⁵⁷H. F. Dobebe, M. Rowekamp, and B. Ruckle, *IEEE J. Quantum Electron.* **QE-20**, 1284 (1984).
- ⁵⁸J. C. White, *IEEE J. Quantum Electron.* **QE-20**, 185 (1984).
- ⁵⁹H. Rottke and H. Zacharias, *Optics Comm.* **55**, 87 (1985).
- ⁶⁰G. Black and L. E. Jusinski, *J. Chem. Phys.* **82**, 789 (1985).
- ⁶¹A. C. Provorov, B. P. Stoicheff, and S. C. Wallace, *J. Chem. Phys.* **67**, 5393 (1977).
- ⁶²D. Cossart and T. Bergeman, *J. Chem. Phys.* **65**, 5462 (1976).
- ⁶³J. E. M. Goldsmith, *J. Chem. Phys.* **78**, 1610 (1983).
- ⁶⁴B. H. Mahan, *J. Chem. Phys.* **33**, 959 (1960).
- ⁶⁵P. Warneck, *J. Chem. Phys.* **41**, 3435 (1964).
- ⁶⁶T. G. Slanger, *J. Chem. Phys.* **45**, 4127 (1966); T. G. Slanger and G. Black, *ibid.* **54**, 1889 (1971).
- ⁶⁷E. C. Y. Inn, *J. Geophys. Res.* **77**, 1991 (1972).
- ⁶⁸T. G. Slanger, R. L. Sharpless, G. Black, and S. V. Filseth, *J. Chem. Phys.* **61**, 5022 (1974).
- ⁶⁹T. G. Slanger and G. Black, *J. Chem. Phys.* **68**, 1844 (1978).
- ⁷⁰C. Strauss, G. McBane, P. L. Houston, I. Burak, and J. W. Hepburn (unpublished results).
- ⁷¹R. G. W. Norrish and G. Porter, *Proc. Roy. Soc. A* **200**, 284 (1950).
- ⁷²F. J. Wright, *J. Phys. Chem.* **64**, 1648 (1960).
- ⁷³A. B. Callear, *Proc. Roy. Soc. A* **276**, 401 (1963).
- ⁷⁴M. deSorgo, A. J. Yarwood, O. P. Strausz, and H. E. Gunning, *Can. J. Chem.* **43**, 1886 (1965).
- ⁷⁵H. Okabe, *J. Chem. Phys.* **56**, 4381 (1972).
- ⁷⁶L. C. Lee and D. L. Judge, *J. Chem. Phys.* **63**, 2782 (1975).
- ⁷⁷M. C. Addison, C. D. Byrne, and R. J. Donovan, *Chem. Phys. Lett.* **64**, 57 (1979).
- ⁷⁸T. R. Loree, J. H. Clark, K. B. Butterfield, J. L. Lyman, and R. Engleman, *J. Photochem.* **10**, 359 (1979).
- ⁷⁹M. C. Addison, R. J. Donovan, and C. Fotakis, *Chem. Phys. Lett.* **74**, 58 (1980); M. Martin and R. J. Donovan, *J. Photochem.* **18**, 245 (1982).
- ⁸⁰J. E. Butler, W. S. Drozodoski, and J. R. McDonald, *Chem. Phys.* **50**, 413 (1980).
- ⁸¹S. Yang, A. Freedmen, M. Kawasaki, and R. Bersohn, *J. Chem. Phys.* **72**, 4048 (1980).
- ⁸²G. Dornhofer, W. Hack, and W. Langel, *J. Phys. Chem.* **88**, 3060 (1984).
- ⁸³K. T. Wu, *J. Phys. Chem.* **89**, 4617 (1985).
- ⁸⁴V. R. McCrary, R. Lu, D. Zakheim, J. A. Russell, J. B. Halpern, and W. M. Jackson, *J. Chem. Phys.* **83**, 3481 (1985).
- ⁸⁵J. Frey, A. Wodtke, and Y. T. Lee (unpublished data); C. Y. Ng (private communication).
- ⁸⁶H. Kanamori and E. Hirota, *J. Chem. Phys.* **83**, 3901 (1987).
- ⁸⁷I. M. Waller and J. W. Hepburn, *J. Chem. Phys.* **87**, 3261 (1987).
- ⁸⁸W. G. Mankin, M. T. Coffey, D. W. T. Griffith, and S. R. Drayson, *Geophys. Res. Lett.* **6**, 853 (1979).
- ⁸⁹N. D. Sze and M. K. W. Ko, *Atmos. Environ.* **14**, 1223 (1980); N. D. Sze and M. K. W. Ko, *Geophys. Res. Lett.* **8**, 765 (1981).
- ⁹⁰R. N. Rudolph and E. C. Y. Inn, *J. Geophys. Res.* **86**, 9891 (1981).
- ⁹¹K. S. Sidhu, I. G. Csizmadia, O. P. Strausz, and H. E. Gunning, *J. Am. Chem. Soc.* **88**, 2412 (1966).
- ⁹²W. H. Breckenridge and H. Taube, *J. Chem. Phys.* **52**, 1713 (1970); **53**, 1750 (1970).
- ⁹³B. M. Ferro and B. G. Reuben, *Faraday Soc. Trans.* **67**, 2847 (1971).
- ⁹⁴J. A. Joens, *J. Phys. Chem.* **89**, 5366 (1985).
- ⁹⁵P. F. Zittel and L. A. Darnton, *J. Chem. Phys.* **77**, 3464 (1982).
- ⁹⁶P. F. Zittel, L. A. Darnton, and D. D. Little, *J. Chem. Phys.* **79**, 5991 (1983).
- ⁹⁷M. C. Lin, *Chem. Phys.* **7**, 433 (1975).
- ⁹⁸G. Black and R. L. Sharpless, *J. Chem. Phys.* **70**, 5567 (1979).
- ⁹⁹J. K. Rice and J. R. Woodworth, *J. Appl. Phys.* **50**, 4415 (1979).
- ¹⁰⁰G. S. Ondrey, S. Kanfer, and R. Bersohn, *J. Chem. Phys.* **79**, 179 (1983).
- ¹⁰¹J. A. Joens and E. J. Bair, *J. Phys. Chem.* **88**, 6009 (1984).

- ¹⁰²N. Sivakumar, I. Burak, W. -Y. Cheung, J. W. Hepburn, and P. L. Houston, *J. Phys. Chem.* **89**, 3609 (1985).
- ¹⁰³G. E. Hall, N. Sivakumar, P. L. Houston, and I. Burak, *Phys. Rev. Lett.* **56**, 1671 (1986).
- ¹⁰⁴S. Buelow, G. Radhakrishnan, J. Catanzarite, and C. Wittig, *J. Chem. Phys.* **83**, 444 (1985).
- ¹⁰⁵K. Honma and O. Kajimoto, *Chem. Phys. Lett.* **117**, 123 (1985).
- ¹⁰⁶C. Jouvet and B. Soep, *Chem. Phys. Lett.* **96**, 426 (1983).
- ¹⁰⁷W. H. Breckenridge, C. Jouvet, and B. Soep, *J. Chem. Phys.* **84**, 1443 (1986).
- ¹⁰⁸W. J. Marinelli, N. Sivakumar, and P. L. Houston, *J. Phys. Chem.* **88**, 6685 (1984).
- ¹⁰⁹S. C. Wallace and G. Zdasiuk, *Appl. Phys. Lett.* **28**, 449 (1976).
- ¹¹⁰D. J. Bamford, S. V. Filseth, M. F. Foltz, J. W. Hepburn, and C. B. Moore, *J. Chem. Phys.* **82**, 3032 (1985).
- ¹¹¹J. W. Hepburn, D. Klimek, K. Liu, R. G. Macdonald, F. J. Northrup, and J. C. Polanyi, *J. Chem., Phys.* **74**, 6226 (1981).
- ¹¹²J. W. Hepburn, F. J. Northrup, G. L. Ogram, J. M. Williamson, and J. C. Polanyi, *Chem. Phys. Lett.* **85**, 227 (1982).
- ¹¹³R. T. Hodgson, P. P. Sorokin, and J. J. Wynne, *Phys. Rev. Lett.* **32**, 343 (1974).
- ¹¹⁴C. E. Moore, *Atomic Energy Levels I*, NSRDS-NBS (U.S.), **35**, (1970).
- ¹¹⁵G. McBane, G. E. Hall, C. Strauss, P. L. Houston, I. Burak, and J. W. Hepburn, (manuscript in preparation).
- ¹¹⁶N. Van Veen, P. Brewer, P. Das, and R. Bersohn, *J. Chem. Phys.* **79**, 4295 (1983).
- ¹¹⁷G. Herzberg, *Molecular Spectra and Molecular Structure I* (Van Nostrand, New York 1950) p. 208; *Molecular Spectra and Molecular Structure II* (Van Nostrand, New York 1945), p. 174.
- ¹¹⁸M. J. Berry, *Chem. Phys. Lett.* **27**, 73 (1974).
- ¹¹⁹Y. B. Band and K. F. Freed, *Chem. Phys. Lett.* **28**, 328 (1974).
- ¹²⁰Y. B. Band and K. F. Freed, *J. Chem. Phys.* **63**, 3382 (1975).
- ¹²¹C. H. Greene and R. N. Zare, *J. Chem. Phys.* **78**, 6741 (1983).
- ¹²²R. Schinke, *J. Phys. Chem.* **90**, 1742 (1986).
- ¹²³W. L. Weise, M. W. Smith, and B. M. Miles, *NSRDS-NBS (U. S.)*, **22**, 134 (1969).
- ¹²⁴R. N. Zare, *Mol. Photochem.* **4**, 1 (1972).
- ¹²⁵R. Bersohn and S. H. Lin, *Adv. Chem. Phys.* **16**, 67 (1969).
- ¹²⁶R. Schmiedl, H. Dugan, W. Meier, and K. H. Welge, *Z. Phys. A* **304**, 137 (1982).
- ¹²⁷C. Jonah, *J. Chem. Phys.* **55**, 1915 (1971).
- ¹²⁸G. Herzberg and E. Teller, *Z. Phys. Chem. B* **21**, 410 (1933).
- ¹²⁹A. C. Albrecht, *J. Chem. Phys.* **33**, 169 (1960).
- ¹³⁰A. Gedanken and I. Burak, *Chem. Phys. Lett.* **137**, 587 (1987).
- ¹³¹R. Renner, *Z. Phys.* **92**, 172 (1934).
- ¹³²G. E. Hall, N. Sivakumar, D. Chawla, P. L. Houston, and I. Burak, *J. Chem. Phys.* **88**, 3682 (1988).
- ¹³³R. N. Dixon, *J. Chem. Phys.* **85**, 1866 (1986).
- ¹³⁴M. Dubs, U. Bruhlmann, and J. R. Huber, *J. Chem. Phys.* **84**, 3106 (1986).
- ¹³⁵K. -H. Gericke, S. Klee, F. J. Comes, and R. N. Dixon, *J. Chem. Phys.* **85**, 4463 (1986).
- ¹³⁶M. P. Docker, A. Hodgson, and J. P. Simons, *Chem. Phys. Lett.* **128**, 264 (1986); *Faraday Discuss. Chem. Soc.* **82**, 25 (1986).
- ¹³⁷I. Burak, J. W. Hepburn, N. Sivakumar, G. E. Hall, G. Chawla, and P. L. Houston, *J. Chem. Phys.* **86**, 1258 (1987).
- ¹³⁸J. A. Joens, *J. Phys. Chem.* **87**, 4614 (1983).
- ¹³⁹J. A. Joens, *J. Chem. Phys.* **86**, 610 (1987).
- ¹⁴⁰P. S. Julienne, D. Neumann, and M. Krauss, *J. Atmos. Sci.* **20**, 833 (1971).
- ¹⁴¹P. J. Gardner and M. Kasha, *J. Chem. Phys.* **50**, 1543 (1969).
- ¹⁴²N. Sivakumar, Ph. D. Thesis, Cornell University, 1986.
- ¹⁴³G. Black and L. E. Jusinsk, *J. Chem. Phys.* **82**, 789 (1985).
- ¹⁴⁴J. Tatum and J. Watson, *Can. J. Phys.* **49**, 2693 (1971) and references therein.
- ¹⁴⁵U. Buck and H. Meyer, *Phys. Rev. Lett.* **52**, 109 (1984).
- ¹⁴⁶Y. Ono, E. A. Osuch, and C. Y. Ng, *J. Chem. Phys.* **74**, 1645 (1981).
- ¹⁴⁷G. Radhakrishnan, S. Buelow, and C. Wittig, *J. Chem. Phys.* **84**, 727 (1986).
- ¹⁴⁸S. Buelow, M. Noble, G. Radhakrishnan, C. Wittig, and G. Hancock, *J. Phys. Chem.* **90**, 1015 (1986).